Developmental Biology 499 (2023) 59–74

Contents lists available at ScienceDirect

Developmental Biology

journal homepage: www.elsevier.com/locate/developmentalbiology

Rab11 is essential to pancreas morphogenesis, lumen formation and endocrine mass

Haley R. Barlow [a], Neha Ahuja [a], Tyler Bierschenk [a], Yadanar Htike [a], Luke Fassetta [a], D. Berfin Azizoglu [b], Juan Flores [c], Nan Gao [c], Sean De la O [d], Julie B. Sneddon [d], Denise K. Marciano [e], Ondine Cleaver [a,*]

[a] Department of Molecular Biology, Center for Regenerative Science and Medicine, USA
[b] Department of Developmental Biology, Beckman Center, 279 W. Campus Drive, B300, Stanford, CA, 94305, USA
[c] Rutgers University Microbiome Program, 679 Hoes Lane West, Piscataway, NJ, 08854, USA
[d] Department of Cell and Tissue Biology, Department of Anatomy, Diabetes Center, Eli and Edythe Broad Center of Regeneration Medicine and Stem Cell Research, University of California, San Francisco, San Francisco, CA, 94143, USA
[e] Internal Medicine and Nephrology, University of Texas Southwestern Medical Center, 5323 Harry Hines Blvd., Dallas, TX, 75390, USA

ARTICLE INFO

Keywords:
Rab11
Pancreas
Epithelium
Cell polarity
Cell shape
Lumen formation
AMIS
Mucin-1
Endocrine cell
Par3/6
Crbs3

ABSTRACT

The molecular links between tissue-level morphogenesis and the differentiation of cell lineages in the pancreas remain elusive despite a decade of studies. We previously showed that in pancreas both processes depend on proper lumenogenesis. The Rab GTPase Rab11 is essential for epithelial lumen formation *in vitro*, however few studies have addressed its functions *in vivo* and none have tested its requirement in pancreas. Here, we show that Rab11 is critical for proper pancreas development. Co-deletion of the Rab11 isoforms *Rab11A* and *Rab11B* in the developing pancreatic epithelium ($Rab11^{pancDKO}$) results in ~50% neonatal lethality and surviving adult $Rab11^{pancDKO}$ mice exhibit defective endocrine function. Loss of both Rab11A and Rab11B in the embryonic pancreas results in morphogenetic defects of the epithelium, including defective lumen formation and lumen interconnection. In contrast to wildtype cells, $Rab11^{pancDKO}$ cells initiate the formation of multiple ectopic lumens, resulting in a failure to coordinate a single apical membrane initiation site (AMIS) between groups of cells. This results in an inability to form ducts with continuous lumens. Here, we show that these defects are due to failures in vesicle trafficking, as apical and junctional components remain trapped within $Rab11^{pancDKO}$ cells. Together, these observations suggest that Rab11 directly regulates epithelial lumen formation and morphogenesis. Our report links intracellular trafficking to organ morphogenesis *in vivo* and presents a novel framework for decoding pancreatic development.

1. Introduction

Lumen formation is a critical process in multicellular organism development, as tubular structures allow for the distribution of gases and liquids deep into organs and tissues. Indeed, the formation of a lumen within a tubular structure is the functional rate-limiting step in the formation of many organ systems including the kidney, lung and cardiovascular systems. Somewhat surprisingly, different tissues utilize different cellular strategies to form lumens (Andrew and Ewald, 2010; Marciano, 2017). Lumens can form by cavitation (e.g. pro-amniotic lumen) (Meng et al., 2017); entrapment (e.g. *Drosophila* heart) (Rugendorff et al., 1994); wrapping (e.g. neural tube formation) (Harland, 1994); cell hollowing (e.g. Drosophila trachea) (Samakovlis et al., 1996); or cord hollowing, in which multiple cells coordinate to target apical proteins to a central location and form a lumen (e.g. initial aortic lumen) (Strilic et al., 2009). Probing the molecular mechanisms driving lumen formation *in vivo* will likely be critical to therapeutic efforts to grow human tissue *ex vivo* for replacement therapies, since the presence and proper organization of lumens is essential to the function of organs (Ryan and Cleaver, 2022).

The cord-hollowing, or *de novo,* mechanism of lumen formation has been observed in organ systems including the cardiovascular system, the

* Corresponding author. Department of Molecular Biology, University of Texas Southwestern Medical Center, 5323 Harry Hines Blvd., NA8.300, Dallas, TX, 75390-9148, USA.
E-mail addresses: haley.barlow@utsouthwestern.edu (H.R. Barlow), ondine.cleaver@utsouthwestern.edu (O. Cleaver).

https://doi.org/10.1016/j.ydbio.2023.05.002
Received 17 November 2022; Received in revised form 21 April 2023; Accepted 9 May 2023
Available online 10 May 2023

kidney, and the pancreas (Gao et al., 2017; Strilic et al., 2009; Villasenor et al., 2010). However, the molecular machinery underlying *de novo* lumen formation has been most thoroughly examined *in vitro* using Madin Darby Canine Kidney (MDCK) cells (Bryant et al., 2010). In this system, a new single central lumen was shown to be initiated between cells following the coordination of a single apical membrane initiation site (termed AMIS) (Bryant et al., 2010). AMIS formation is a dynamic process, as membrane-associated proteins are rapidly moved to and from various locations as cells acquire polarity. Apically and basally localized proteins are trafficked, junctions are rearranged, cell shape is changed, and the cytoskeleton undergoes rapid and dynamic changes to support these processes. Moreover, components of polarity determining complexes such as the Par (apical), Crumbs (apical) and Scribble (basolateral) complexes are known to contribute to AMIS formation (Overeem et al., 2015). These complexes regulate strong positive feedback loops that maintain the distinct identities of the apical and basolateral membranes (for further review see Roman-Fernandez and Bryant (2016)). Although much is known about AMIS and lumen formation in cultured cells, molecules that drive polarity acquisition and subsequent lumen formation in developing mammalian tissues remain largely unexplored.

The developing murine pancreas presents an opportunity to study *de novo* lumen formation *in vivo*. The pancreatic epithelium first buds from the foregut endoderm as a stratified epithelial placode around embryonic day (E) 8.75 (Flasse et al., 2021; Pictet et al., 1972; Slack, 1995; Villasenor et al., 2010). Within this multilayered epithelium, *de novo* microlumens emerge in the initial, unbranched pancreas (Braitsch et al., 2019; Villasenor et al., 2010). These microlumens, which initially emerge individually between epithelial cells, go on to connect to each other to form a highly interconnected three-dimensional lumenal plexus that also connects to the foregut lumen (Hick et al., 2009; Kesavan et al., 2009; Villasenor et al., 2010). This net-like lumen network expands in size as the pancreas grows and fully ramifies after birth into a branched, glandular epithelial tree. It is within this plexus that endocrine progenitors are born (Bankaitis et al., 2015). Unlike in other organ systems, *de novo* lumenogenesis continues to occur alongside lumen remodeling and extension as the pancreas grows, and only ceases at birth.

How are these dynamic cellular activities executed and coordinated? Here, we focus on how vesicle-mediated recycling regulates membrane and protein trafficking during lumen formation and pancreas morphogenesis. Specifically, we focus on the master of membrane recycling Rab11 (Rab11A and Rab11B). Rab11 is a member of the Ras superfamily of GTPases that is known to regulate secretory and endocytic vesicular trafficking, including recycling of several membrane surface proteins (Goldenring et al., 1996; Ossipova et al., 2014; Zhang et al., 2021). Rab11 has been shown to regulate cell polarity and cell division in yeast and zebrafish (Tanasic et al., 2022) as well as lumen formation in MDCK cells (Desclozeaux et al., 2008; Hales et al., 2002; Neto et al., 2013; Overeem et al., 2015; Rathbun et al., 2020; Roland et al., 2011). During MDCK lumen formation, Rab11 localizes at the AMIS and traffics proteins from the basal to the apical membrane, as cells establish polarity. In the absence of Rab11, MDCK lumen formation is disrupted (Bryant et al., 2010; Desclozeaux et al., 2008). These observations established Rab11 as an important regulator of polarity determination and lumen formation in cultured epithelial cells. However, there has been surprisingly little examination of the role of Rab11 during mammalian *in vivo* lumen formation. Our studies previously implicated Rab11 in pancreatic lumen formation *in vivo* (Azizoglu et al., 2017). In the absence of the junction-associated scaffolding protein Afadin, the formation and organization of epithelial lumens in the pancreas is severely disrupted. Loss of Afadin leads to the disruption of Rab11 localization and to a concomitant accumulation of intracellular cargo containing both apical and junctional components. Based on these observations, we asked how Rab11 might regulate pancreatic lumen formation *in vivo*.

To our knowledge, the present study is the first to characterize ablation of Rab11 (Rab11A and Rab11B) *in vivo* during organogenesis, and to identify functional links between vesicle trafficking, polarity acquisition, lumen formation, and tissue morphogenesis (Lapierre et al., 2003). Here we show that loss of Rab11 in the mouse pancreatic epithelium leads to postnatal lethality and defective pancreatic endocrine function. These deficiencies are linked to fetal pancreatic hypoplasia and a decrease in endocrine cell mass. Furthermore, the loss of Rab11 leads to profound epithelial morphogenetic defects. In the $Rab11^{pancDKO}$ pancreas at E14.5, nascent lumens fail to form or to connect and build a plexus, as apical and lumenal proteins remain trapped inside epithelial cells. $Rab11^{pancDKO}$ cells also display severely disrupted polarity and often participate in formation of more than one AMIS between neighbors. These defects are associated with mislocalization of Par and Crumbs polarity complex proteins, as well as the tight junction component ZO-1. We propose that Rab11 is required in the pancreatic epithelium *in vivo* for the formation of a single AMIS that subsequently matures into a single coordinated lumen. When these processes are disrupted, the morphogenesis of the pancreas is defective, and endocrine cell fate is affected. Together, these findings identify cellular and molecular mechanisms underlying pancreatic morphogenesis and underscore the functional connections between lumen formation and epithelial morphogenesis.

2. Results

2.1. Rab11 is expressed in the developing mouse pancreas

We previously showed that the junctional protein Afadin was required for epithelial lumen formation, as well as for the normal localization of Rab GTPases and for the proper pancreas development (Azizoglu et al., 2017). Notably, lumen disruption upon Afadin loss was accompanied by dramatic subcellular mislocalization of Rab11 in pancreatic epithelial cells. In this study, we assess whether Rab11 is involved in pancreas development.

We first assessed expression of Rab11A and Rab11B transcripts and proteins throughout pancreatic development, both transcriptionally and by protein expression. *In situ* hybridization for *Rab11a* and *Rab11b* suggested that expression was both ubiquitous and low in the pancreas for both genes (Fig. S1 A,C). We also examined public databases of mRNA expression and found similar results (Genepaint, https://gp3.mpg.de/) (Fig. S1 B,D). Similarly, analysis of single-cell RNA-sequencing data showed that *Rab11a* and *Rab11b* were expressed in all pancreatic lineages throughout pancreas development (Fig. S1 E-G, data derived from (Byrnes et al., 2018)) and in adults (Fig. S1H, data from Tabula Muris https://tabula-muris.ds.czbiohub.org/).

Assessing expression of Rab11A by immunofluorescence (IF), we found that at all stages examined (embryonic day (E) 10.5, E11.5, E12.5, E14.5, E18.5), it was enriched at the center of epithelial rosettes (previously described in Villasenor et al. (2010)) and ducts. Specifically, we observed Rab11A enrichment at the apical membrane of 'pre-lumens' (or AMIS, Fig. 1 A'; red arrows), nascent lumens (Fig. 1 B′,C'; yellow arrows) and established lumens (Fig. 1 D'; green arrow, **F-G′**). As developmental time progressed, we observed an increase in signal intensity and coordination of localization towards the apical membrane as lumens matured (Fig. 1 E). Localization of Rab11B was not assessed, as there is currently no effective Rab11B antibody available for IF.

We also evaluated expression of Rab11A in the three primary pancreatic epithelial lineages – acinar, ductal and endocrine. At E18.5, we found Rab11A largely restricted to the apical membranes of both acinar and ductal cells (Fig. 1 F-G'; Fig. S2 A-B′, D,D′), while exhibiting low expression in endocrine cells (Fig. 1 H,H'; Fig. S2 C-D′). We confirmed the localization of Rab11A in the three main pancreatic epithelial lineages at E18.5 both by epithelial morphology (Fig. 1 F–H'; Fig. S2 D,D′) and by analysis of lineage-specific markers carboxypeptidase A1 (CPA1) (acinar; Fig. S2 A,A′), Sox9 (ductal; Fig. S2 B,B′), and Insulin and Glucagon (endocrine; Fig. S2 C,C′). Note strong lumen localization at the center of epithelial rosettes (acinus, a) and along the apical aspect of duct epithelium (duct, d), while scattered punctate

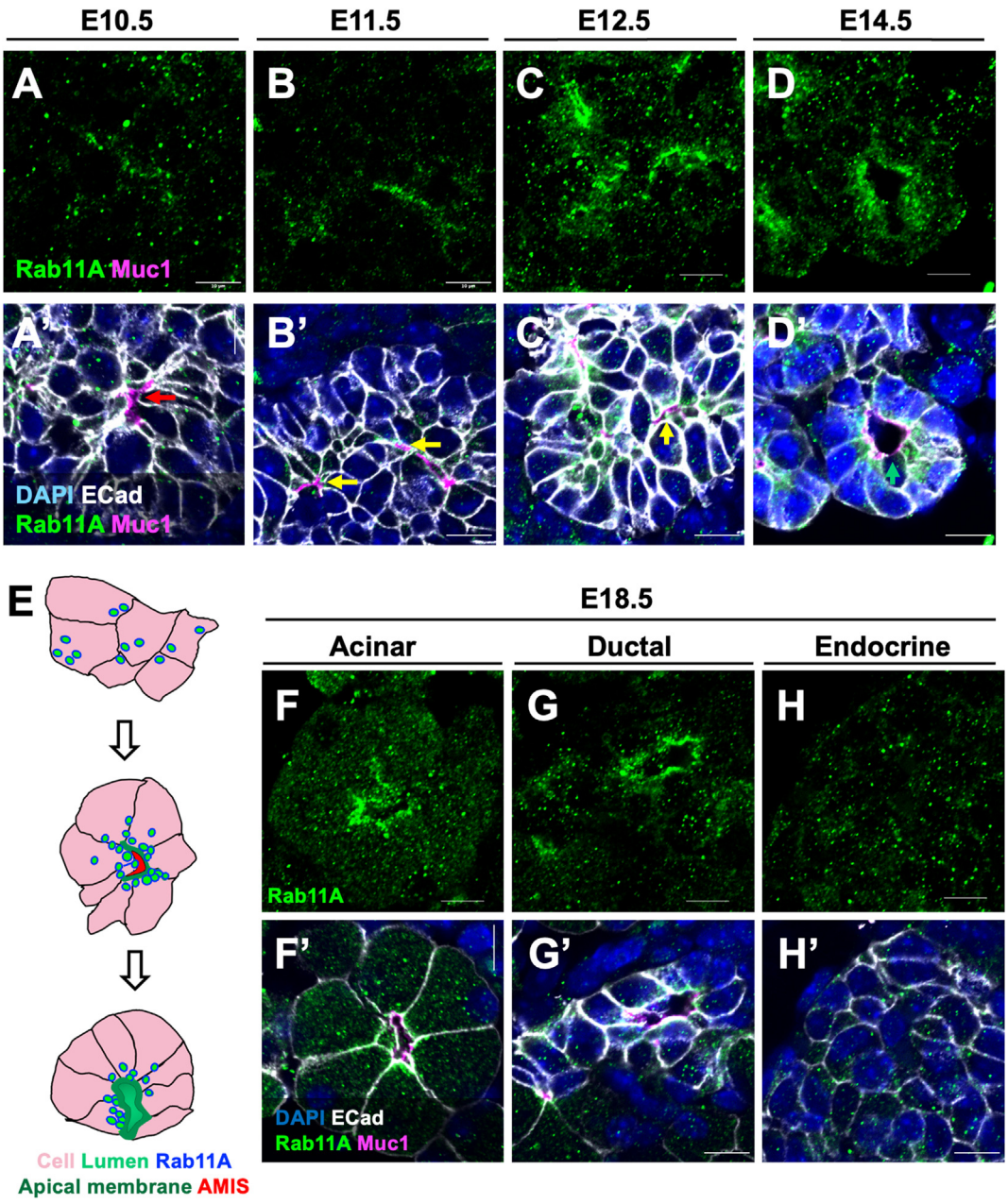

Fig. 1. Vesicle-mediated recycling regulator Rab11 localizes to lumens throughout pancreatic development. (A–D) Rab11A protein (green) is enriched at apical membranes (Muc1, magenta) of developing AMIS sites at early- **(A-C′)** and mid-gestational **(D-D′)** stages of pancreatic development. Note Muc1 marking pre-lumens at E10.5 and E11.5 (**A′,B'**; red arrows); nascent lumens at E12.5 (**B′, C'**; yellow arrow); and established lumens at E14.5 (**D'**; green arrow). **(E)** Schematic representing the shift in localization of Rab11A protein as *de novo* lumens form, where epithelial cells are depicted in pink, Rab11A^{+} vesicles in bright green, Apical Membrane Initiation Site (AMIS) in red, apical membrane in dark green, and the open lumen is green. **(F–H′)** At E18.5, Rab11A localization remains restricted to apical membranes of lumens at the center of epithelial rosettes **(F,F′)** in acinar cells and **(G,G′)** ductal cells. **(H,H′)** Endocrine cells also display lower levels of Rab11A expression. n>3, scale bars = 10 μm throughout.

expression in endocrine cells (islet, i) (Fig. S2 D'; dotted yellow lines). Alternative immunostaining methods were used to enhance IF signal, and to detect lateral localization of Rab11A in ductal cells (Fig. S2 B,B'), however this was not observed using other staining methods. Overall, these results support the idea that Rab11A is a strong candidate regulator of pancreatic lumen formation.

2.2. Loss of pancreatic Rab11 results in postnatal lethality and glucose clearance defects

To assess a potential role of Rab11 during pancreas development, we genetically ablated *Rab11a* from the pancreatic epithelium utilizing the *Pdx1-Cre* driver in a *Rab11b*-null background (*Rab11*^{pancDKO}) (Hingorani et al., 2003; Yu et al., 2014b). *Rab11a*$^{f/f}$; *Rab11b*$^{-/-}$ females were crossed to *Pdx1-Cre* expressing males that were heterozygous either for *Rab11a* or *Rab11b* (*Rab11a*$^{f/+}$;*Rab11b*$^{-/-}$ or *Rab11a*$^{f/f}$;*Rab11b*$^{+/-}$) and harbored a copy of *Pdx1-Cre*. Individual mutants of *Rab11a* or *Rab11b* did not display any noticeable phenotype and were therefore included in the pool of controls for all experiments, and the breeding of heterozygous males indicated above were viable and fertile with no obvious abnormalities. *Rab11a* deletion in *Rab11*^{pancDKO} mice was confirmed by testing the presence of Rab11A protein via immunostaining in the midgestational E14.5 pancreatic epithelium (Fig. S3 A-B").

Expected ratios of mutants were observed during embryonic

development. However, when we allowed pregnant dams to give birth, we found that only approximately half of the mutant animals survived, with the most common survival time being to postnatal day (P) 2 (Fig. 2 A). By postnatal day 8 (P8), surviving *Rab11*^{pancDKO} pups largely displayed no significant differences in size quantified by body length and body weight, although there was a trend towards lower body weights (Fig. S4 A,B). A small but notable number of runted *Rab11*^{pancDKO} pups survived past P2 and displayed failure to thrive (Fig. 2 B).

When 6-week adult animals were subjected to a glucose tolerance test (GTT), surviving *Rab11*^{pancDKO} animals showed impaired glucose clearance (Fig. 2 C). We noted that females displayed increased peak levels of glucose levels within the first hour following glucose injection, and it took them longer to return to normal blood glucose levels, indicating that endocrine function impairment is more significant in females. Interestingly, we also found that variability in *Rab11*^{pancDKO} adult animal weight and size was most pronounced in females, although there was no significant difference in either measurement (Fig. S4 C-E). Visualization of blood glucose measurements as violin plots also revealed a dramatic variability in phenotype severity of surviving *Rab11*^{pancDKO} mice, in both males and females (Fig. S4 F). These results suggest that both Rab11A and Rab11B are required for full proper function of the adult mouse pancreas. We also note that since neither individual mutant alone displayed defects, both Rab11A and Rab11B likely are needed together for optimal function, either via redundancy or complimentary additive functions.

2.3. *Rab11*^{pancDKO} exhibit pancreas hypoplasia and epithelial defects

To assess the underlying cause of low survival rate and abnormal endocrine function in Rab11 mutant mice, we examined the pancreata of E18.5 and P2 mutants. Upon dissection of the midgut organs such as the stomach, duodenum and pancreas, we observed clear defects in *Rab11*-^{pancDKO} pancreata (Fig. 3A and B), accompanied by a statistically significant decrease in pancreas weight (Fig. 3 C). In addition to a smaller epithelial mass, the pancreas was less branched and some large cysts in the pancreatic epithelium were observed (Fig. 3 A-C, S5 F–I', **S6 A-C,** yellow arrowheads). This hypoplasia was specific to the pancreas, as the overall size of E18.5 *Rab11*^{pancDKO} embryos was the same as their control littermates (Fig. S5 E).

Given that our primary interest in studying Rab11 was understanding its role in developmental dynamics, we examined developing pancreata at earlier stages. At both E12.5 and E14.5, we observed no externally obvious defects (Fig. 3 D-F; Fig. S5 A-D) and the epithelial volume of the pancreas (as measured with IMARIS software) in *Rab11*^{pancDKO} and controls was roughly equivalent at E14.5, albeit with a trend towards decreased size in the mutant pancreata (Fig. 3 F). Upon examination of E14.5 mutant pancreata in section, we found that the epithelium and the acini at the tips of branches exhibited clear morphogenetic differences in the mutants (Fig. 3 D-F and Fig. S5 A-D). Acinar cells can be recognized by their anatomical location at the tips of ductal branches, which form florets of approximately 8–12 acinar cells around a central lumen, but also by their expression of the acinar cell marker CPA1 (Fig. 3G, H).

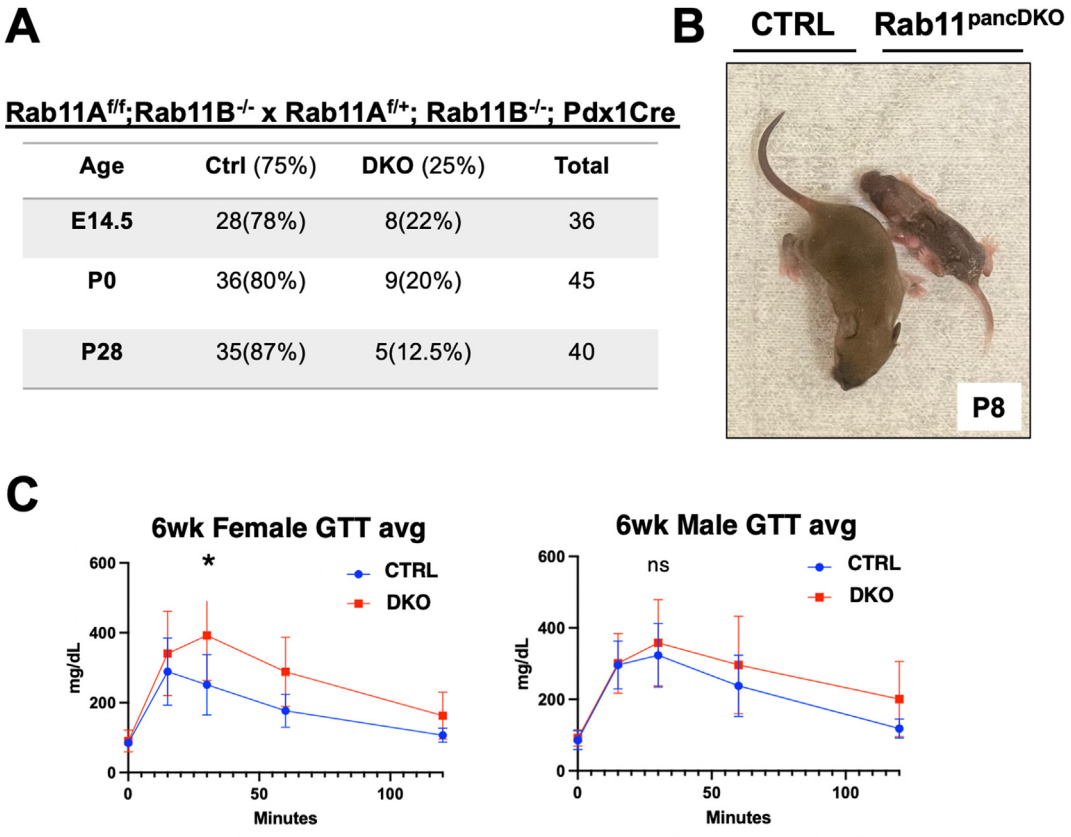

Fig. 2. Loss of Rab11 leads to postnatal lethality and mild defects in adult endocrine function. **(A)** *Rab11*^{pancDKO} mutants are present during gestation and at birth at expected ratios. However, approximately half of *Rab11*^{pancDKO} mutants die before weaning. **(B)** Surviving mutants were generally the same size and length as their control littermates, with occasional mutants being smaller. **(C)** Control and surviving *Rab11*^{pancDKO} mice were tested for their ability to clear blood glucose with a glucose tolerance test, or GTT (a test for endocrine function). Both females and males were tested. We found that mutant males exhibited mildly impaired glucose clearance, while mutant females displayed significantly higher peak glucose levels. n = 111 mice analyzed for survival; n>3 mutants that fail to thrive postnatally; n = 8 female mice (4 control/4 mutant) and n = 8 male mice (4 control/4 mutant) per group for adult GTT analyses. Data analyzed in PRISM by 2-way ANOVA.

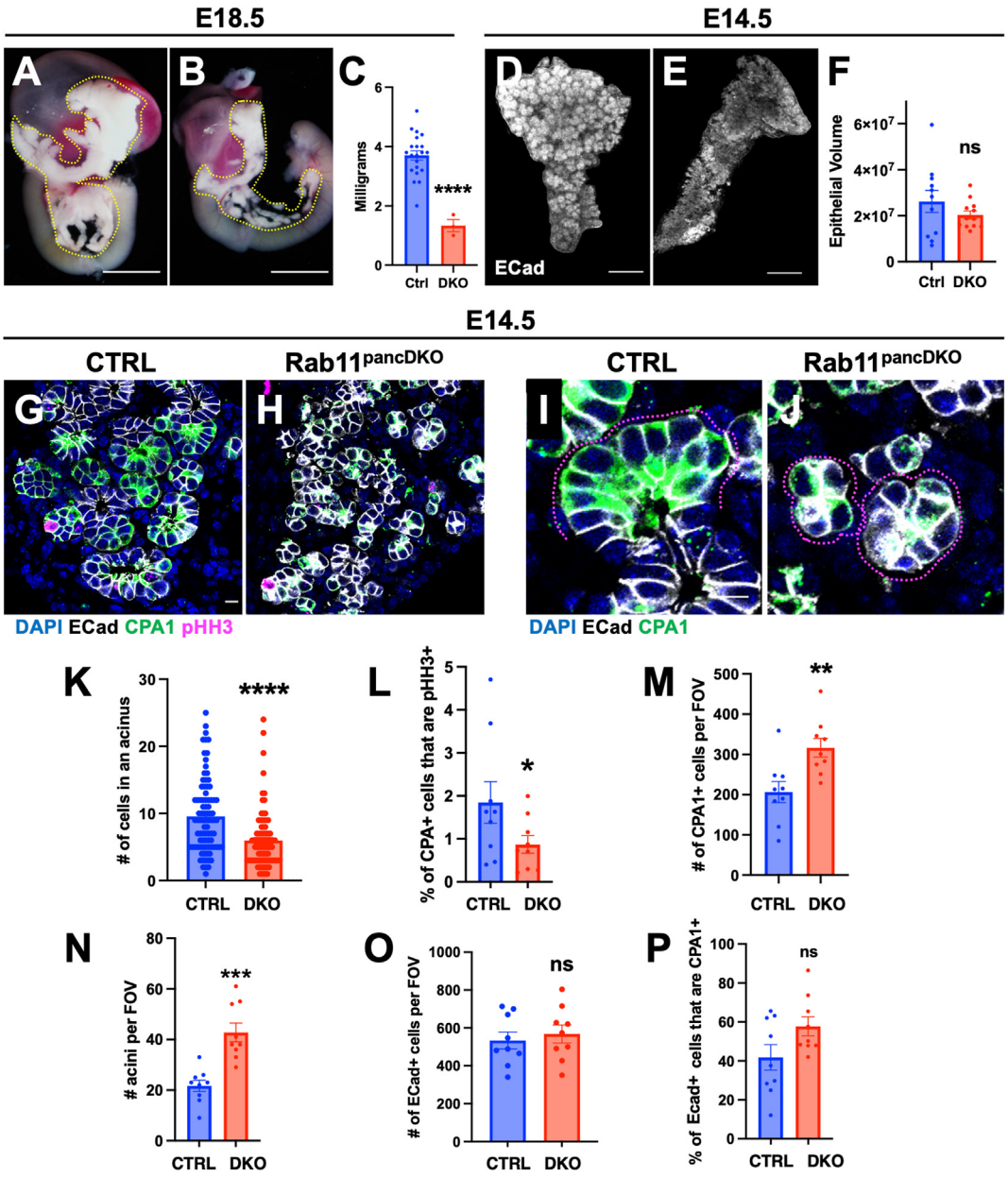

Fig. 3. Loss of Rab11 leads to disruption of overall epithelial morphogenesis. (A,B) At E18.5, morphogenetic defects are present in the hypoplastic *Rab11*^{pancDKO} pancreas compared to a littermate control (pancreas, yellow dotted line), **(C)** accompanied by a decrease in pancreas weight. **(D–F)** At E14.5, there is a non-significant trend towards a decrease in epithelial volume in mutants as shown in whole mount with staining for ECad (white) to mark pancreatic epithelium. **(G,H)** In tissue sections at E14.5, clear morphogenetic defects are visible in the pancreatic epithelium (ECad, white). **(I,J)** Higher magnification view reveals that acinar cell morphogenesis is defective (CPA1, green; individual acini are outlined in magenta). **(K)** A significant decrease in the number of acinar cells per acinus in mutants is associated with a decrease in acinar cell proliferation (**G,H,L**; pHH3, magenta). Surprisingly, this is associated with an increase in both the number of acinar cells and the number of acini at E14.5 per field of view (FOV) in the *Rab11*^{pancDKO} pancreata **(M,N)**, while the total number of ECad^{+} cells per FOV is unchanged **(O)**. **(P)** The total percentage of ECad^{+} cells that are also CPA1^{+} is not significantly increased. n>3 for E18.5, n ≥ 8 for ECad volumes, n = 3 for CPA1 stains; error bars represent the standard error of the mean throughout; scale bars A-B = 0.5 cm, D-E = 200 μm, G-J = 20 μm; data analyzed in PRISM by a Student's t-test.

Mutant acinar cells could also be recognized by the expression of CPA1, however the morphology and organization of these cells were abnormal (Fig. 3 I, J).

Given the defects in the size of mutant pancreata, and the known role of Rab11 in epithelial cell division (Dong et al., 2017), we sought to examine whether cell proliferation rates might be affected by the absence of Rab11. Indeed, we noted that unlike acini in controls, the Rab11 mutants exhibited acini with strikingly fewer cells than controls (Fig. 3 H, J). Quantification of these rosette-like structures in the *Rab11*^{pancDKO} pancreas revealed on average 50% fewer acinar cells per acinus (control average = ~9; *Rab11*^{pancDKO} average = ~5) (Fig. 3 K), and this was associated with a decrease in acinar cell proliferation in the mutants (Fig. 3 G,H, L; Fig. S6 D-J). Seemingly in contrast, both the number of acinar cells and the number of acini per field of view (FOV) increased despite decreased proliferation rates (Fig. 3M and N). We also found that the density of epithelial tissue was unchanged in the mutants (Fig. 3 O), as was the overall proliferation rate of the epithelium containing both exocrine (ductal and acinar) and endocrine cells (Fig. S6 J). These findings suggest that the *Rab11*^{pancDKO} epithelium is undergoing aberrant morphogenesis, generating many more, but smaller, acinar tips per FOV. Indeed, it is worth pointing out that the overall organ in mutants tended to be slightly smaller, hence the overall number of acinar cells in the

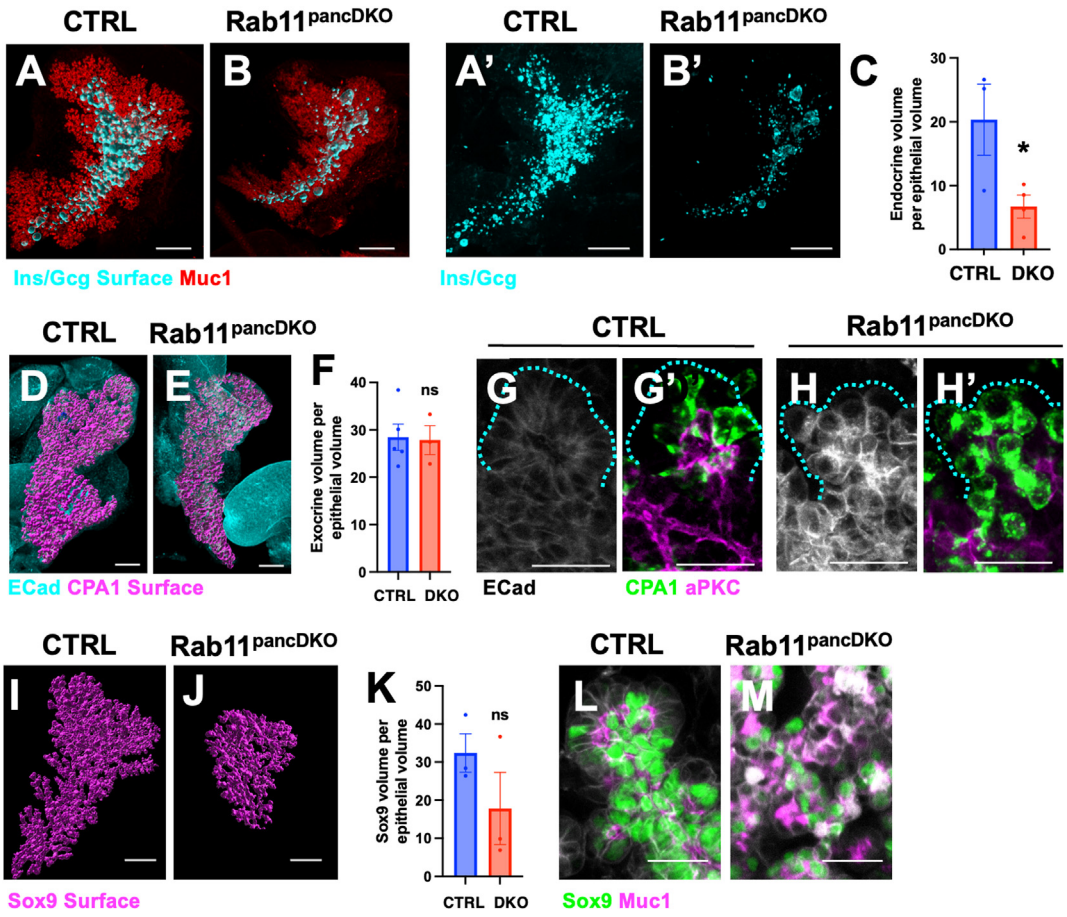

Fig. 4. Loss of Rab11 leads to loss of ducto-endocrine mass. To assess changes in cell fate determination, control and mutant E14.5 pancreata were analyzed in whole mount. At E14.5, there is a clear decrease in endocrine volume (Insulin/Glucagon, cyan; **(A,B)** IMARIS surface, Muc1 red; **(A′,B′)** whole mount staining). **(C)** Even when accounting for the trend in decrease in epithelial volume decrease in *Rab11*^{pancDKO} pancreata, there is a statistically significant decrease in endocrine volume (μm^3). In analyzing other pancreatic lineages in a similar way, we found that there is no detectable change in exocrine volume (CPA1, magenta) **(D-F)**, although as seen in **(G′, H′)**, the organization of CPA1$^+$ cells (green) around lumenal tips (outlined in cyan) is disrupted **(G-H′)** (ECad, white; aPKC, magenta; CPA1, green). **(I,J)** *Rab11*^{pancDKO} display a non-significant trend of decreased volume of ductal Sox9. **(I,J)** Sox9 IMARIS surface, magenta. Quantification of **(I,J)** in **(K)**. **(L,M)** Similar to our findings regarding exocrine cell organization, Sox9$^+$ cells (green) that are destined to contribute to a ductal fate are disorganized in the *Rab11*^{pancDKO} **(L,M)**. n = 3, error bars represent the standard error of the mean; scale bars A-B' = 200 μm, D,E, I,J = 150 μm, G-H′, L,M = 20 μm; data analyzed in PRISM by Student's t-test.

entire gland was not likely higher (Figs. 3 P, Fig. 4 D-F). Rather, it is the morphogenetic branching of the pancreas that is altered in the absence of Rab11.

2.4. Loss of Rab11 leads to loss of endocrine mass

Following our analysis of the morphologically altered acinar lineage in the *Rab11*^{pancDKO} mutant pancreas, we next asked whether the differentiation of the ductal and endocrine lineages was altered. Using whole mount immunofluorescence staining of both control littermate and *Rab11*^{pancDKO} pancreata, we found that the volume of endocrine cells (Insulin$^+$ and Glucagon$^+$) per epithelial volume was altogether decreased in E14.5 pancreata in the absence of Rab11 (Fig. 4 A-C). The loss of endocrine mass impacted some areas of the pancreas more than others (Fig. S7 A-C, and panel 1). Interestingly, we observed a significant decrease in the number of endocrine progenitors, as per staining for the endocrine progenitor marker Neurogenin3 (Neurog3 or Ngn3) and pancreatic duodenal homeobox 1 (Pdx1) (Fig. S7 D-I, panel 2), suggesting a possible failure in endocrine cell differentiation. Further characterization of islets in controls and mutants at adult stages showed that there was no differential loss in the number of Insulin versus Glucagon cells or vice versa (Fig. S7 J-O). Indeed, islets themselves showed few abnormalizes, as they contained all expected relative numbers of endocrine cell types, and their organization was grossly normal (i.e. inner core of beta cells surrounded by glucagon + cells and other endocrine cell types).

Consistent with our analysis of CPA1$^+$ exocrine cell fate from (Fig. 3 P) in section, we did not detect a significant difference between the volume or density of CPA1$^+$ cells per epithelial volume in whole mount at E14.5 (Fig. 4 D-F). Since the overall size of the pancreas is reduced at perinatal stages (Fig. 3A–C, and Fig. S5 F–I), a defect in exocrine tissue expansion must occur prior to these stages. Indeed, we observed organizational defects in acini as early as E14.5 (Fig. 3 G-J). CPA1$^+$ acinar cells are primarily restricted to the ends of epithelial branches in controls, but this organization was severely disrupted in the mutants (Fig. 4 G-H'). In examining ductal cell fate, we did not detect a significant change in the volume of Sox9$^+$ cells per epithelial volume (Fig. 4 I–K) despite a tendency towards reduced volume. However, organizational disruption was clearly present in this cell population as well (Fig. 4L and M). Overall, we found that the organization and morphogenesis of the pancreatic epithelium in the *Rab11*^{pancDKO} is severely disrupted, and this disruption is correlated with a decrease in endocrine volume. This decrease in endocrine mass may contribute to the defective endocrine function seen in adult mice in (Fig. 2 C).

2.5. Rab11 is necessary for the formation of a lumenal network in the pancreas

Given the known role of Rab11 in MDCK epithelial lumen formation (Bryant et al., 2010) and the mislocalization of Rab11 that is observed in lumen-defective Afadin pancreatic mutants (Azizoglu et al., 2017), we sought to understand the role of Rab11 in pancreatic lumenogenesis. Using whole mount immunostaining of pancreatic lumens for the lumenal protein Mucin-1 (Muc1), we observed dramatic defects in the formation of the pancreatic lumenal plexus. As early as E14.5, *Rab11-^{pancDKO}* lumens have less distinct boundaries than controls and fail to connect to each other properly (Fig. 5 A-B′). Furthermore, there are very few obvious ductal structures (Fig. 5 B,B'). These changes are represented as a model in (Fig. 5 C). When observed at a higher magnification, lumens in control tissues have well-defined borders and are clearly connected. Although it is normal to see some fuzzy lumen-associated protein in some cells. By contrast, the mutant lumens display very few lumens with well-defined borders, connections are unclear and most of the Muc1 signal has indistinct borders. Indeed, quantification of the number of disconnected lumens in IMARIS revealed a significant increase in the number of disconnected lumens per total epithelial volume in *Rab11-^{pancDKO}* tissues (Fig. 5 D).

At E18.5, we found that the lumens had progressed dramatically in two different directions: either as small disconnected microlumens, or as connected but swollen cystic lumens (Fig. 5 E-F'). We believe that residual lumens are likely due to incomplete deletion of *Rab11a* and *Rab11b*, as some of the epithelial cells lining these cystic lumens retained expression of Rab11A (Fig. S8). This cystic phenotype was particularly surprising given that most of the acini of the pancreas were not connected to these ducts; one might expect smaller, more constricted ducts due to the presumed decrease in fluid volume. Overall, the data suggest that Rab11 plays an integral role in the formation and organization of the lumenal plexus in the developing pancreas.

2.6. Loss of Rab11 leads to defects in secretion of apical cargo

We next assessed *Rab11^{pancDKO}* pancreata in sections to determine why the mutant lumens were disconnected from each other. Looking more closely at *Rab11^{pancDKO}* tissue at both E14.5 and E18.5, we found that mutant tissues had severe morphogenetic defects that were associated with disconnected lumens (Fig. 6 A-D). Indeed, the failure of lumen continuity appears to derive from a primary failure of lumen formation, both at E14.5 (Fig. 6A,B) and E18.5 (Fig. 6C,D).

Upon examination of E14.5 mutant epithelial cells, apically-secreted protein Muc1 was observed trapped inside *Rab11^{pancDKO}* mutant cells compared to controls (Fig. 6 E-F′). This resulted in loss of lumen boundary distinction in whole mount stained pancreas tissue. Similarly, we noted that the adherens junction protein E-Cadherin (ECad)

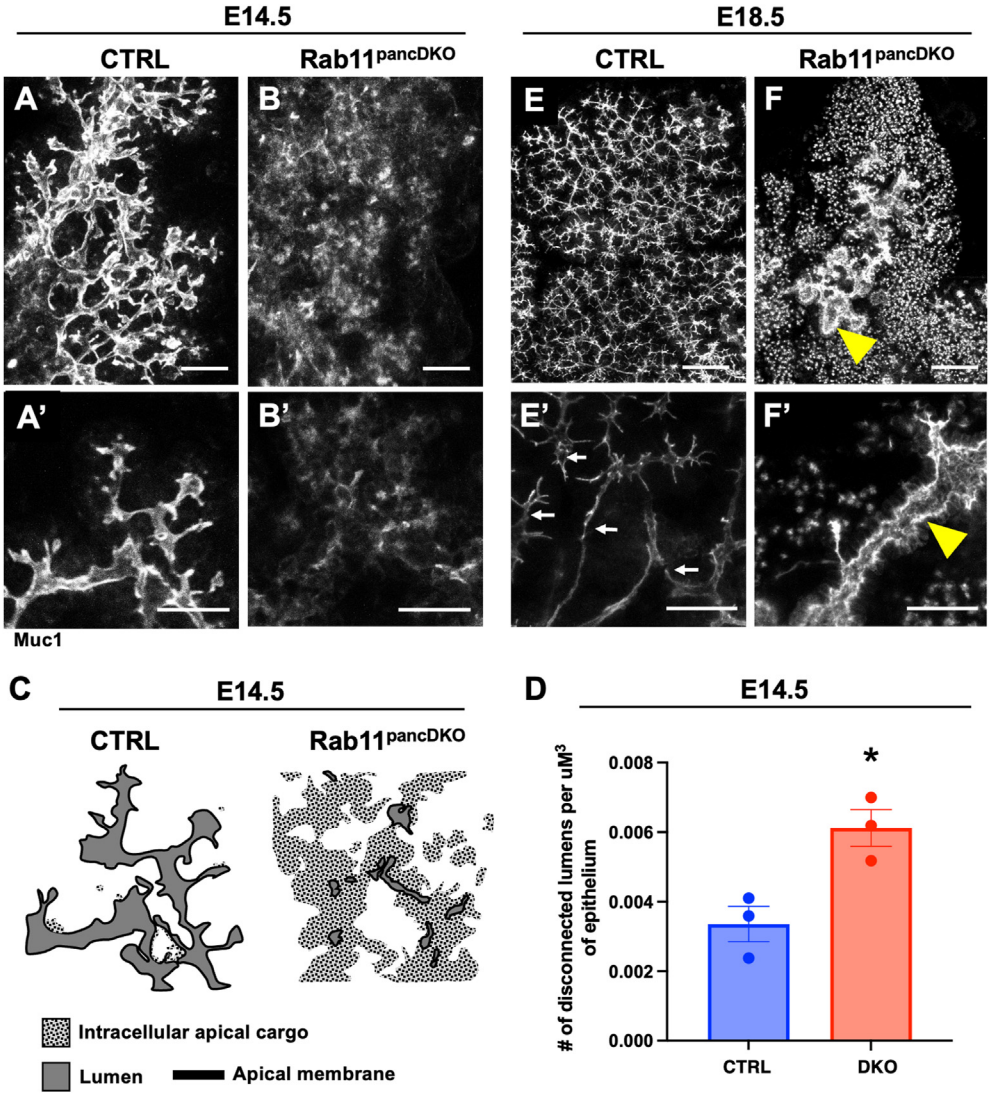

Fig. 5. Rab11A and Rab11B are essential for the formation of the pancreatic lumenal plexus. (A,A′) At E14.5, control pancreata have complex lumenal networks as shown in whole mount (Muc1, white). **(B,B′)** In *Rab11^{pancDKO}* mutants, maximum intensity projections of the same tissue thickness show indistinct lumen borders and an apparent lack of organization. **(A′)** Higher resolution images of thinner stacks show well-connected lumens in control tissues, while **(B′)** mutant lumens are largely not connected and display fuzzy, indistinct borders. **(E,E′)** At E18.5, control lumens remain distinct and connected (Muc1, white), while **(F,F′)** *Rab11^{pancDKO}* mutants display a combination of disconnected microlumens and large cyst-like connected lumens. **(E′,F′)** Higher resolution images show connected lumens with distinct boundaries in control tissue (white arrowheads), while the mutant lumens are either small, disconnected dots or swollen cyst-like ductal structures **(F,F′** yellow arrowheads**).** The shift away from clear and connected lumens with very few regions of indistinct intracellular cargo is represented in schematic **(C),** where lumens are dark grey surrounded by black apical membrane, and intracellular cargo are light grey with black speckles representing apical membrane. **(D)** A statistically significant increase in the number of disconnected lumens per total lumen volume is observed at E14.5. n = 3 for all experiments; error bars represent the standard error of the mean; scale bars A-D = 25 μm, E,F = 100 μm, E′,F′ = 50 μm; data in **(D)** analyzed in PRISM by a Student's t-test.

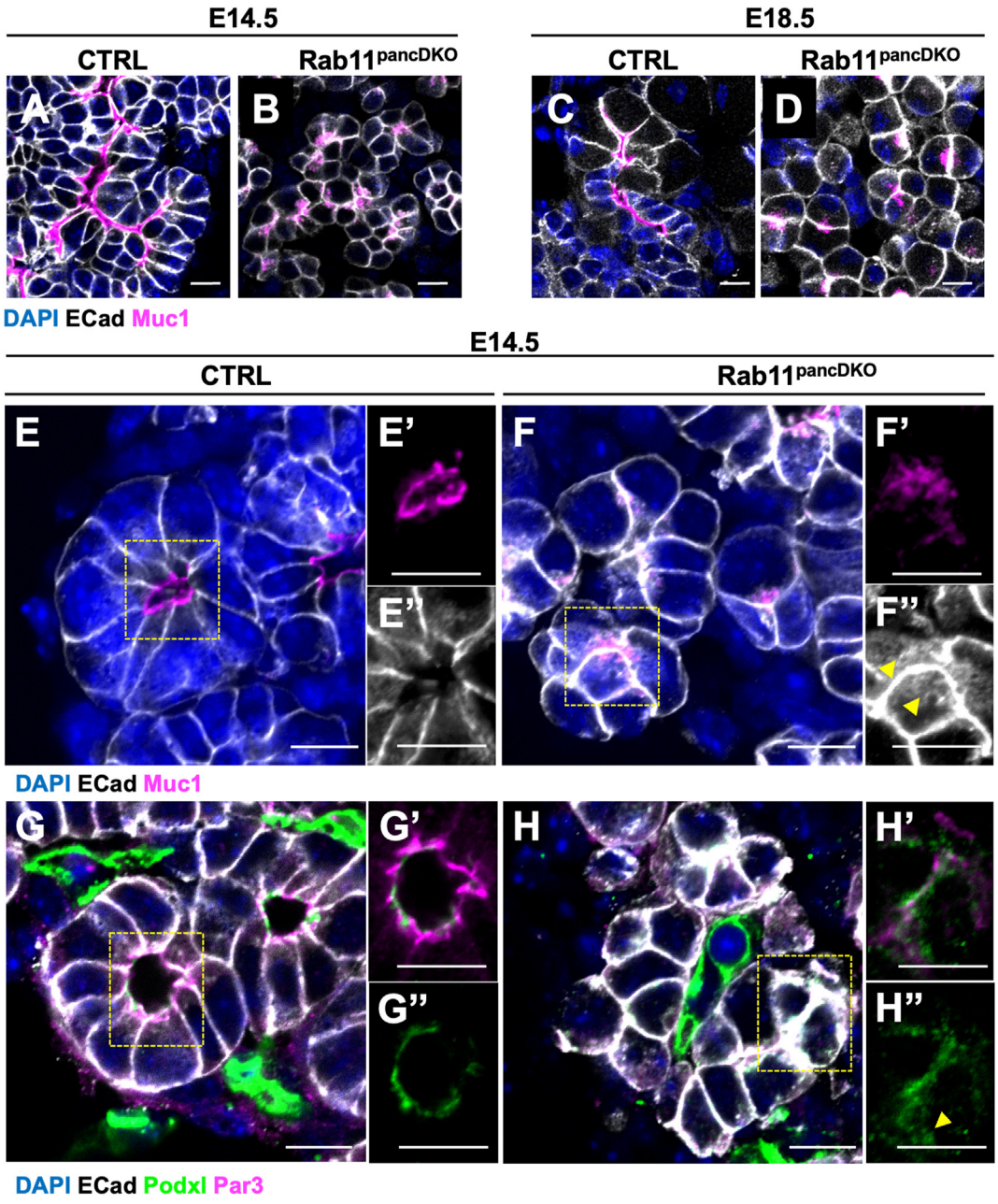

Fig. 6. Loss of Rab11 leads to retention of apically-targeted cargo. Sections through pancreatic tissue at both E14.5 **(A,B)** and E18.5 **(C,D)** show changes in epithelial morphology (ECad, white) as well as lumen connectivity (Muc1, magenta; DAPI, blue). **(E)** Upon closer examination, E14.5 control tissue displays clear open lumens (Muc1, magenta) with distinct boundaries and an apical membrane region **(E′)** that largely excludes ECad (white) **(E″). (F,F′)** *Rab11*^{pancDKO} tissue instead shows intracellular retention of lumen marker Muc1 (magenta) that correlates with a failure of lumen formation. **(F″)** Trafficking failures are further confirmed by the strong presence of ECad around each cell border, even where lumen marker Muc1 is localized. An increase in intracellular ECad is observed (yellow arrowheads), including along presumptive apical ends of cells. **(G-G″)** Lumen marker Podxl (green) is similarly localized to the apical membrane (Par3, magenta) in open lumens in control tissue, but is mislocalized within the cytoplasm (yellow arrowheads) in *Rab11*^{pancDKO} tissue **(H–H″)** (insets indicated in yellow dotted lines). n = 4 for A-D; n>3 for E-F"; n = 3 for G-H"; scale bars = 10 μm, yellow boxes indicate regions from which insets are generated for the following panels.

localization shifted upon loss of Rab11, resulting in an increase in intracellular retention of ECad (Fig. 6 E″,F″, yellow arrowheads). In addition, Ecad could also be observed at presumptive apical surfaces of cells (Fig. 6 F″). Note in wildtype cells, apical surfaces of epithelial cells are devoid of Ecad (Fig. 6 E"). Furthermore Podocalyxin (Podxl), a protein that both marks and facilitates the formation of lumens, was similarly trapped inside cells (yellow arrowhead) (Fig. 6 G-H″), or sometimes undetectable (data not shown). These findings suggest that Rab11 is critically required for faithful trafficking of required components during AMIS formation.

2.7. *Rab11*^{pancDKO} *cells exhibit abnormal cell polarization*

Given that proper transport of cellular elements is critical to establishment and maintenance of cell polarity (Roman-Fernandez and Bryant, 2016), we further investigated the localization of apical and basal components in *Rab11*^{pancDKO} epithelial cells. As shown in (Fig. 6), we had noted intracellular retention of Muc1. We also found that there was mislocalization of Muc1 to the lateral or even the basal membrane in some cells (Fig. 7 A-B′, white asterisks). Some mutant cells seemed to make more than one AMIS (two different areas of Muc1 accumulation

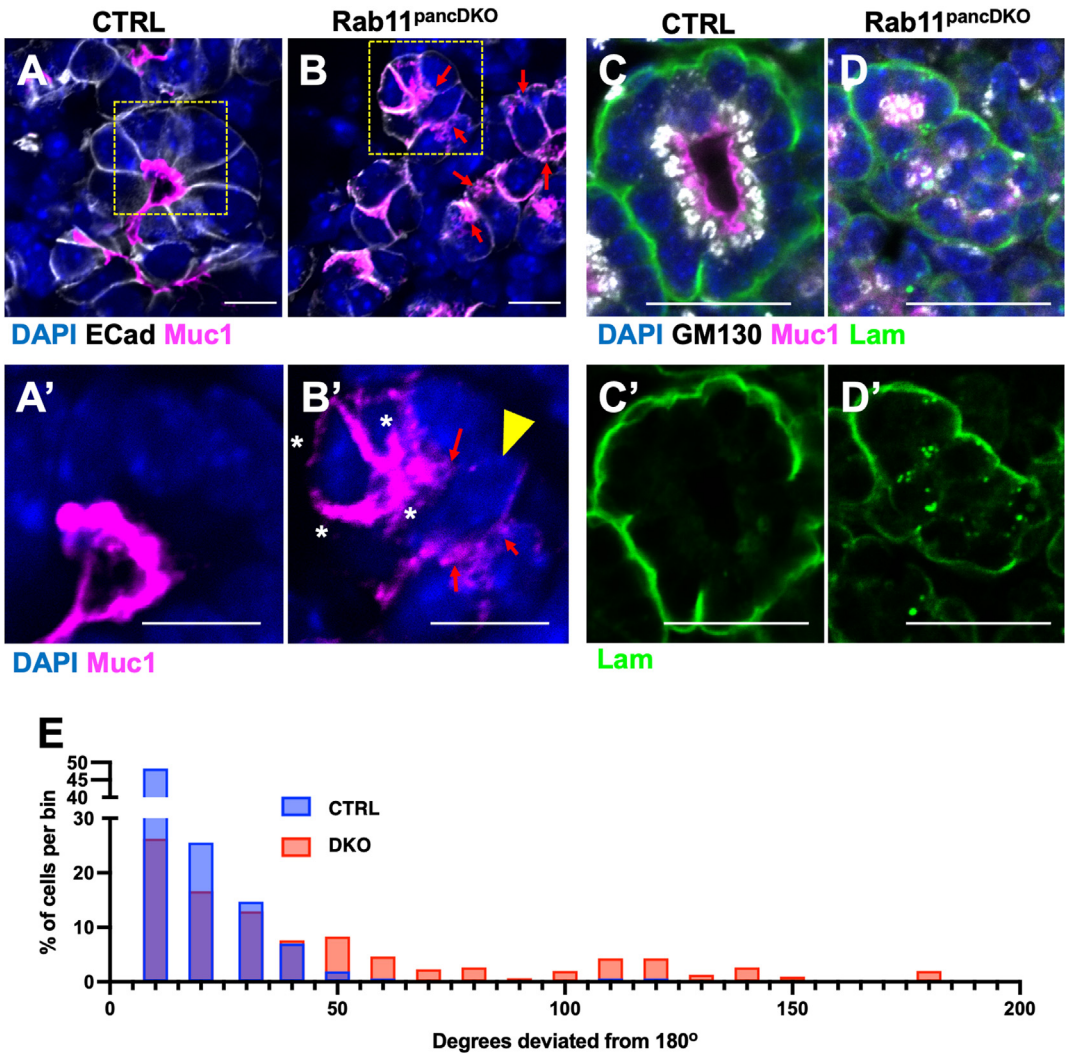

Fig. 7. ***Rab11*^{pancDKO} cells exhibit abnormal cell polarization**. In contrast to control tissue where most cells have a single apical membrane (**A**, yellow box; **A′**), *Rab11*^{pancDKO} mutant cells display apical markers (Muc1, magenta) on multiple membranes (**B**, yellow box; **B′**, white asterisks indicate multiple Muc1+ membranes) and/or participate in multiple apical sites (**B′**, yellow arrowhead indicates cell with multiple apical sites, which are shown by red arrows). To assess overall cell polarity, control and *Rab11*^{pancDKO} tissues were stained for basement membrane (Laminin, green), nuclei (DAPI, blue), Golgi (GM130, white) and apical membrane (Muc1, magenta) **(C,D)**. **(E)** To measure cell polarity, we calculated a 'polarity index' by measuring in FIJI the angles created by lines drawn from basement membrane to Golgi (through the nucleus, yellow line), and from the Golgi to the apical membrane. The deviation of each measurement from a "perfectly" polarized cell represented by a 180° angle was calculated and binned into 10° deviation categories. **(E)** Plotting the % of total cells per bin revealed a clear shift in cell polarity in mutants. Of note, there also seems to be defects in trafficking Laminin in mutant cells (D′). n>3 for A-B'; n = 3 for C-E; scale bars = 10 μm.

flanking a single cell), thus participating in more than one attempt to form lumens between neighbors (Fig. 7 B′, note single cell, yellow arrowhead, that has multiple AMIS, red arrows).

This observation led us to examine the overall polarity of these cells by staining E14.5 sections for Laminin (basal extracellular matrix), GM130 (Golgi), Muc1 (apical membrane) and DAPI (nucleus) (Fig. 7 C-D′). We found that *Rab11*^{pancDKO} cells displayed both punctate internal laminin staining (Fig. 7 D′), as well as abnormally localized GM130 (Fig. 7 C-D,E). To quantify potential defects in cell polarity, we generated a 'polarity index' by drawing a line in FIJI from the basal membrane through the nucleus to the Golgi, and drawing another line from the Golgi to the apical membrane. The angle formed by these two lines was quantified and compared between controls and mutants, with the assumption that an angle of 180° (a straight line) would represent a perfectly polarized cell (see materials and methods). There was a clear shift in the distribution of polarity angles away from 180° in the mutant cells, with some cells even displaying angles that are never seen in control cells (including 0°, indicating cells whose basal and apical membranes overlap) (quantification Fig. 7 E). Overall, *Rab11*^{pancDKO} cells frequently display severely altered cell polarity.

2.8. *Rab11 is required for the coordination of a single AMIS*

We next asked whether polarity-determining proteins such as members of the Par (Par6b, Par3, aPKC) or Crumbs (Crbs3) complexes were mislocalized in the *Rab11*^{pancDKO} cells, as has been previously reported in other systems (Bryant et al., 2010; Rathbun et al., 2020) Indeed, although some of each polarity protein assayed was able to incorporate into an AMIS, there was an increase in intracellular signal from each protein, as well as a significant increase in the number of apical sites per cell in the mutants (Fig. 8 A-H′,K,L). This reflects the localization of apically-targeted proteins to multiple regions of the cell membrane shown in (Fig. 7 B,B'); in other words, loss of Rab11A and Rab11B results in the formation of multiple AMIS per epithelial rosette. The tight junction protein ZO-1 largely followed the localization of apical membrane in *Rab11*^{pancDKO} cells, but we also observed instances where there were tight junctions both within and between cells where there was no apical membrane present (Fig. 8 I-L).

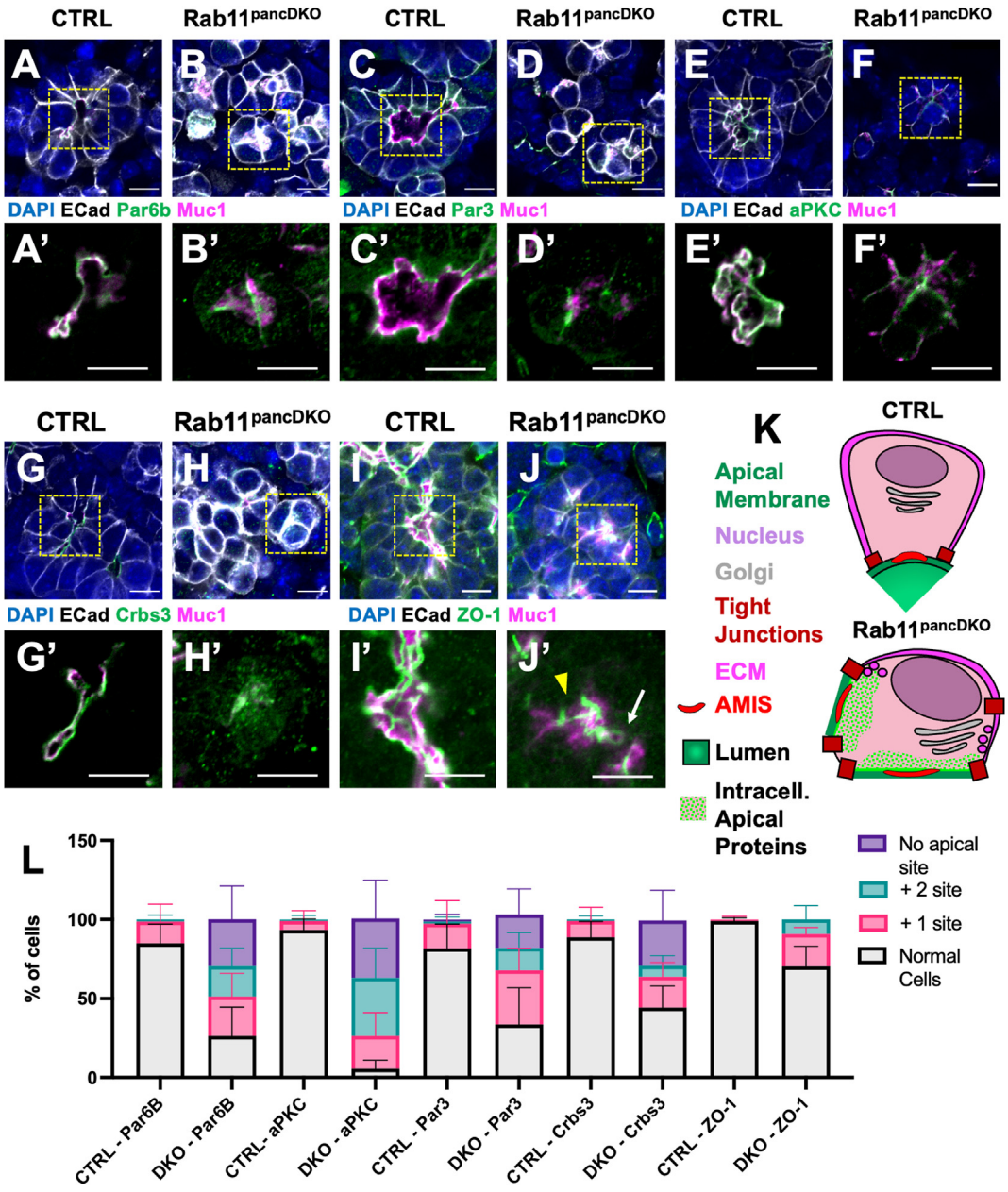

Fig. 8. Rab11 is required for the coordination of a single apical membrane initiation site (AMIS). Localization of apical polarity determining Par complex **(A-F′)** and Crumbs complex **(G-H′)** markers were assessed in control and *Rab11*^{pancDKO} tissue. Immunofluorescence for **(A-B′)** Par6b, **(C-D′)** Par3, and **(E-F′)** aPKC (green) localized tightly to the apical membrane (Muc1, magenta) in control tissue. **(B′, D′, F′)** In *Rab11*^{pancDKO} tissue, a fraction of each of these Par complex components were able to properly localize to the apical membrane, but many mutant cells displayed intracellularly-retained polarity markers, as well as the formation of multiple apical sites per cell. Similarly, Crumbs complex member Crumbs3 (**G-H′** green) is tightly localized to the apical membrane (Muc1, magenta) in control tissue **(G,G′)**, while intracellular retention of Crbs3 is increased in the *Rab11*^{pancDKO} **(H,H′). (I,I′)** Furthermore, tight junction marker ZO-1 (magenta) localizes to cell-cell contacts beneath the apical membrane (aPKC, green) in control tissue. In mutant tissue, ZO-1 continues to associate with regions of apical membranes, but is also ectopically present within (**J′**, white arrow) or between (**J′**, yellow arrowhead) cells that are not coordinating an AMIS (**J,J′**). A model summarizing the defects found in Figs. 7 and 8 is shown in **(K)** (AMIS, red; cell, pink; laminin/ECM, magenta; nucleus, periwinkle; Golgi, grey; ZO1, dark red; apical polarity determining complex proteins, dark green; lumen, light green). The percent of cells that have ectopic apical sites as indicated by Par6b, Par3, aPKC, Crbs3 or ZO-1 staining are quantified in **(L)**. There is no significant difference ($p>0.05$) between the percentage of cells with 1 extra Par6B site, with 1 extra aPKC site, with 2 extra Par3 sites, or with 1 or 2 extra Crbs3 sites. There is also no significant difference between ZO-1 levels. There is a highly significant difference ($0.001>p>0.0001$) between the percentage of cells with 2 extra Par6B sites and with no Par3 sites. There is a highly significant difference ($p<0.0001$) between the percentage of cells with a single Par6B site, with no Par6B site, with a single aPKC site, with 2 extra aPKC sites, with no aPKC site, with a single Par3 site, with a single Crbs3 site, and with no Crbs3 site. N = 3; scale bars = 10 μm; data in (L) were analyzed by a 2-way ANOVA with multiple comparisons in PRISM.

These data suggest that Rab11 is critical for the coordination of a single AMIS between groups of cells by affecting the localization of polarity-determining proteins. Our findings from (Fig. 7) and (Fig. 8) are summarized in (Fig. 8 K), where in the mutant cells the Golgi (grey) is improperly oriented, multiple AMIS (red) form, junctions (red) are mistargeted, and both apical (green) and basal (magenta) components are retained intracellularly. Given these observations, it is no surprise that pancreatic morphogenesis is so severely disrupted in the *Rab11-*^{pancDKO}, and that endocrine cells that are born within the early pancreatic plexus are impaired. Altogether, our results suggest that Rab11 regulates

initial molecular composition and localization of lumens, via localization of apical membrane initiation sites (AMIS), and that it is therefore essential for overall pancreas morphogenesis and function via its crucial role in lumen formation.

3. Discussion

Here we report that loss of Rab11A and Rab11B (*Rab11*^{pancDKO}) in the developing mouse pancreas results in defects in pancreatic morphogenesis that are linked to the failure of single AMIS and lumen formation. Ablation of either Rab11A or Rab11B alone does not result in pancreatic defects. These are novel findings because AMIS formation and subsequent single lumen formation has primarily been studied in *in vitro* systems in which lumens are being formed between two cells. In the developing pancreas and in other developing organs, lumens are instead formed between groups of cells. Previous models of *de novo* lumen formation have not considered the unique organizational needs of larger groups of cells. In the absence of Rab11, cells form multiple AMIS and fail to coordinately form a single central lumen. As a result, the pancreatic epithelium fails to establish the connected lumenal plexus. These lumen formation defects are linked to dramatic changes in pancreatic morphogenesis. The *Rab11*^{pancDKO} pancreata also display a decrease in endocrine cell mass, which is likely linked to the defects in ductal plexus formation and morphogenesis (as we previously showed in Azizoglu et al. (2017)). This study underscores the stark requirement for Rab11 during pancreas development, and specifically shows that Rab11 is essential for epithelial lumen formation during organogenesis.

3.1. Rab11 and vesicle trafficking

Our work, together with decades of in *vitro* molecular studies of Rab11 and of vesicle trafficking in general (Ren et al., 1998; Stenmark and Olkkonen, 2001) allow us to speculate as to why loss of Rab11 may so profoundly impair murine pancreas development. The primary molecular function of Rab11 is to facilitate recycling of various cargoes around the cell. It has been shown by others that Rab11 helps vesicles bud off the recycling endosome and targets them to the correct region of the plasma membrane via coordination with Rab8 and Myosin5B (Bryant

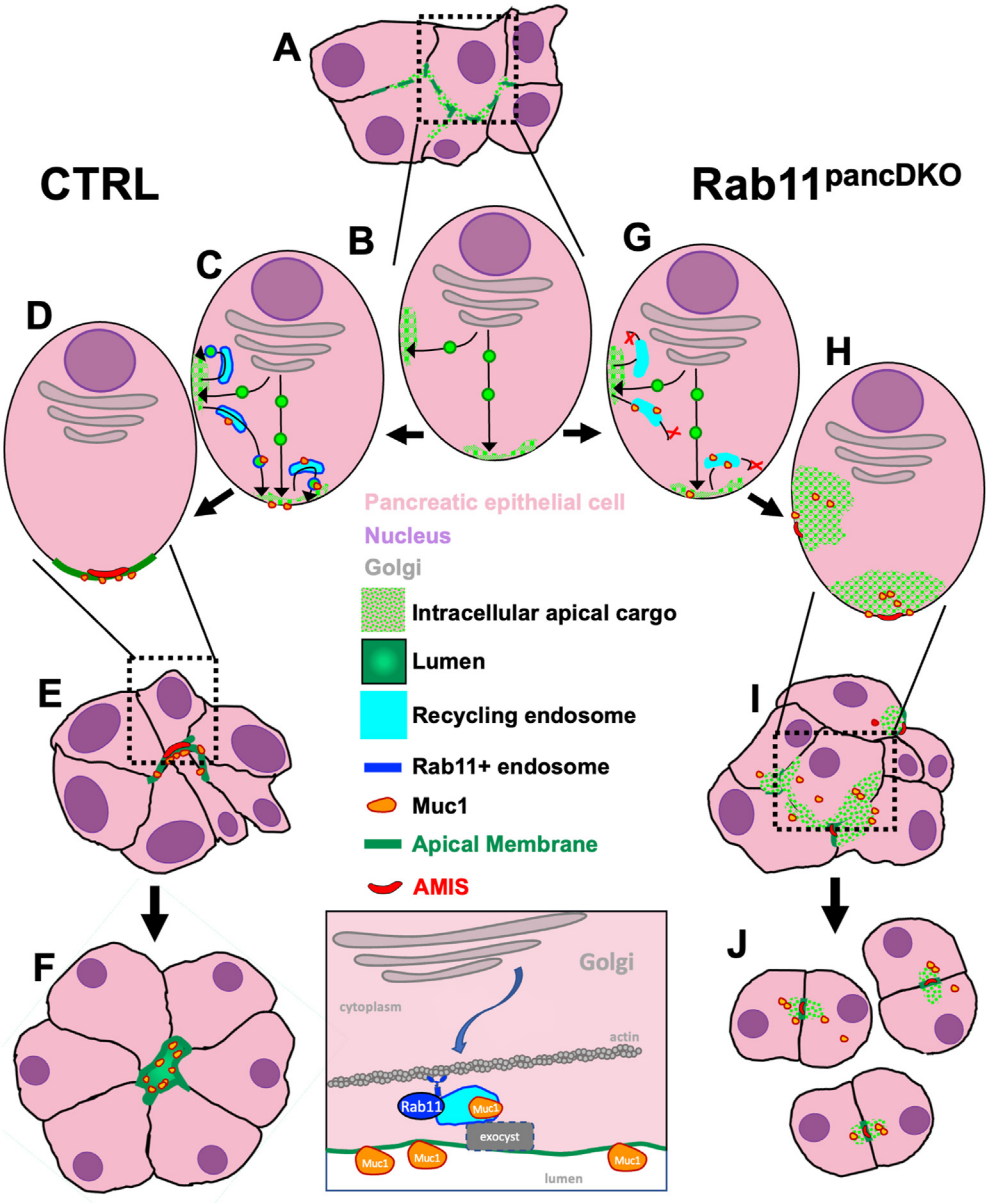

Fig. 9. Model: Rab11 directs the formation of a singular apical membrane initiation site through the proper membrane-localization of apical and junctional proteins. (A) During early stages of pancreatic development, stratified epithelial cells have not yet coordinated a single AMIS, and there is often more intracellular apical cargo in wild-type cells compared to later stages of pancreas development. **(B)** Based on the known roles and functions of Rab11 from other studies, we propose that in the pancreatic epithelium Rab11 directs and enables recycling of apical and junctional components. **(C,D)** In particular, we propose that Rab11 regulates: 1. normal turnover of membrane-associated proteins such as Muc1 at both the lateral and apical membranes (this could also be true of basal proteins, but our study focused on the apical side of the cell), and 2. re-localization of proteins from the lateral membrane to the apical membrane, thus orchestrating a single AMIS. **(E,F)** WT pancreatic epithelial cells continue to traffic and exocytose various proteins, enabling the cells to open a single lumen between themselves. **(G)** We propose that the redirection of recycling membrane is disrupted in *Rab11*^{pancDKO} cells. **(H)** Apical and junctional proteins are still trafficked to the apical and lateral membranes, but after uptake of membrane for either normal turnover or lateral-to-apical re-localization, proteins are unable to return to the membrane in the absence of Rab11. **(H,I)** This leads to the formation of multiple apical sites per cell and a failure to clear adherens junction protein ECad from the apical membrane. **(J)** By morphogenetic processes still unclear, mutant midgestational pancreatic cells are able to shift from multicellular aggregates to primarily two-cell wide structures surrounding a single AMIS whose necessary apical proteins are trapped inside each cell. Pancreatic epithelial cells, pink; AMIS, red; apical membrane, green; exocyst, dark grey; nucleus, purple; Golgi, grey; intracellular apical cargo, bright green spots on a pink background; lumen, green; Muc1, orange; recycling endosomes, blue.

et al., 2010; Hales et al., 2002; Roland et al., 2011). This process has been closely studied at the apical membrane, but Rab11 is also known to traffic cargoes such as E-Cadherin and integrins to and from the lateral and basal membranes, respectively (Desclozeaux et al., 2008; Moreno et al., 2022; Tanasic et al., 2022; Woichansky et al., 2016). Indeed, we speculate that Rab11 recycling of lateral membrane cargo to the apical membrane, as well as its role in promoting apical membrane turnover, are both critical to lumen formation (Fig. 9).

3.2. Membrane remodeling by Rab11 during morphogenesis

Together, our findings in this study led us to propose the following model: Rab11 normally drives regular turnover at both the lateral and apical membranes, as well as redirection of proteins from the lateral to the apical membrane. Tight regulation of these trafficking movements allows cells to coordinate in the formation of a single AMIS (Fig. 9 A-D) that then expands into an open lumen (Fig. 9 D-F). In the *Rab11*^{pancDKO} pancreatic epithelium, cells are capable of initiating polarity formation, AMIS formation, and lumen formation (Fig. 9 B,G), however we speculate that loss of Rab11 blocks the redirection of membrane and proteins out of the recycling endosome back to the plasma membrane, resulting in cells that are unable to drive lumenogenesis across the finish line (Fig. 9G and H). We propose that proteins and membrane are constantly turned over and sorted through the recycling endosomes, but in the absence of Rab11 they cannot be properly targeted back to the plasma membrane (Fig. 9G and H). This phenomenon may drive the intracellular buildup of apical and junctional cargo in the *Rab11*^{pancDKO}, rather than a direct failure of initial targeting and exocytosis.

Our findings that multiple apical sites form in the absence of recycling regulator Rab11 suggest that normal cells may initially target apical components to more than one location in the cell during AMIS formation, only to be "cleaned up" and recycled away from the forming lateral membrane to the apical membrane (Fig. 9C and D). While this hypothesis requires further testing, it may shed some light on how cells accomplish the feat of choosing and coordinating an AMIS in large groups of cells *in vivo* (Fig. 9 A-F). For indeed, in the *Rab11*^{pancDKO} (Fig. 9 F) and in Rab11 knockdown or mutation studies in other systems (Bryant et al., 2010), groups of cells form multiple lumens (or attempt to, in the case of the *Rab11*^{pancDKO}). Upon loss of Rab11, intracellular vesicles tasked with treadmilling and recycling either apical cargo or cell-cell adhesion molecules, normally destined for the apical or lateral membranes, end up accumulating or being inappropriately targeted and resulting in lumens not at the apical membrane, but at ectopic locations between cells. How cells in the *Rab11*^{pancDKO} can largely overcome this multiple-lumen initiation over the course of development, and remodel into pairs of cells with stunted AMIS-like foci and no connected lumen (Fig. 9 I-J), requires further study.

Given our observations, we propose that in many ways pancreatic microlumens form similarly to Madin-Darby Canine Kidney (MDCK) cell lumens, a process extensively studied by the Mostov group and its scientific descendants (Bryant et al., 2010; Flasse et al., 2021; Kim et al., 2015; Mostov and Deitcher, 1986; Pollack et al., 1997, 1998; Roland et al., 2011). A similar mechanism has been proposed for lumen initiation and expansion in tubules of development mouse kidney (Gao et al., 2017). Findings from our lab (Villasenor et al., 2010) and others (Roman-Fernandez and Bryant, 2016) show that, similar to MDCK cells, junctions and apical polarity determining complex proteins, such as the Par complex and the Crumbs complex, are coordinately targeted to a single apical location that is "agreed upon" by all the pancreatic epithelial cells participating in the newly forming lumen. These cells form a three-dimensional (3D) rosette of polarized cells that initiate single lumen formation at their center. The opening of a microlumen is facilitated in part by secretion of negatively-charged Podocalyxin, creating ionic repulsion forces, as well as by actomyosin-generated contractile forces (Camelo and Luschnig, 2021; Dekan et al., 1991; Schottenfeld-Roames et al., 2014; Strilic et al., 2009). Once a pancreatic microlumen has been formed through these mechanisms, it then fuses with other microlumens and with the foregut lumen (Villasenor et al., 2010). Our work shows that some of these events are mediated by Rab11.

Another open question in the field focuses on how junctions are cleared from the AMIS to facilitate detachment of cells during lumen formation. Two possible mechanisms have been proposed: passive or active junction clearance. In the passive junction clearance model, junctional proteins are pushed to the periphery by continuous addition of new membrane lacking junctional proteins to the AMIS. While it is known that there is a switch in apical membrane biogenesis in which junction proteins are no longer added, simply displacing junction proteins from the AMIS may not fully account for their continued restriction to the periphery (Marciano, 2017). In the active model, junction proteins are endocytosed from the AMIS and recycled to the periphery (Flasse et al., 2021; Yan et al., 2016). Our finding that E-Cadherin is retained at the apical membrane upon loss of Rab11 (Fig. 6 F–F″, H–H") suggests that recycling is indeed required to clear junctions from the apical membrane to facilitate lumen opening. This model aligns with active clearance of junctions observed in our previous studies in blood vessel lumen formation that identify active clearance of junctions (Barry et al., 2016). However, our data could be explained by either of the two models.

3.3. Loss of Rab11 reveals dependence of endocrine differentiation on plexus integrity

Our data underscore the direct link between epithelial morphogenesis and both endocrine and exocrine cell fate. In our previous studies, we showed that when the pancreatic epithelium fails to transform from a stratified epithelium to a ramifying tree of continuous ducts containing functional lumens, the emergence of endocrine cells is altered (Azizoglu et al., 2017). In that study, the loss of the protein Afadin and its partner RhoA led to a delay in the resolution of the lumenal plexus, which we postulated resulted in additional cycles of proliferation of endocrine progenitors within the plexus, leading to a near three-fold expansion in endocrine cell mass. Given that Rab11 was mislocalized in the absence of Afadin, we predicted the ablation of Rab11 would yield a similar phenotype. However, in the absence of Rab11 we observe instead the loss of endocrine cells. We ascribe this difference to the different anatomy of the mutant epithelium, whereby rather than large, multi-layered epithelial aggregates observed in *Afadin*^{pancDKO}, we find a breakup of the epithelium into finer structures in the *Rab11*^{pancDKO} (as shown by cross sections showing 2-cell wide strands, Fig. 6 A-D). This finding is reminiscent of the loss of integrity of the pancreatic plexus observed in the *CDC42* pancreas deletion model by the Semb group, in which Ngn3+ cells are significantly reduced in numbers, without a change in detectable cell proliferation (Kesavan et al., 2009). However, in contrast to the *Cdc42*^{pancKO}, we do not observe a compensatory increase in acinar cells. Together, these observations support the existence and fundamental importance of a 3D niche for endocrine development that depends on proper lumen formation. However, it still remains to be seen how and why different plexus morphological abnormalities differentially impacts endocrine progenitor turnover – i.e. increasing endocrine mass in the *Afadin*^{pancKO} (Azizoglu et al., 2017), while decreasing it in the *Cdc42*^{pancKO} (Kesavan et al., 2009) and the *Rab11*^{pancDKO}.

In addition, it is worth noting that loss of Rab11A and Rab11B results in mild effects on glucose tolerance. The mild nature of the defectis is likely because mice are resilient to significant loss of endocrine mass. Mice lacking up to 60% of their pancreas following pancreatectomy survive and show only mild defects in glucose clearance (Peshavaria et al., 2006). Hence, the mild defects that we do observe in our mutant mice may very well reflect relatively significant defects in pancreatic endocrine cells.

3.4. Loss of Rab11 impairs endocrine mass but not cell proliferation

There are other possibilities that should be considered as to what

Rab11 might be doing in pancreatic epithelial cells. Previous studies have tied Rab11 to polarized cell division and proliferation (Dong et al., 2017; Howe et al., 2020). It is also possible that Rab11 might control survival, or function of endocrine cells via their secretory roles (Xu et al., 2011). We did not assess changes in plane of cell division in the mutants, as polarized cell division in epithelial morphogenesis of the developing pancreas is poorly characterized and thus our experimental system currently lacks a strong framework for analyzing the *Rab11*^{pancDKO} phenotype in that context. Future studies that tackle this issue in the tortuous developing pancreatic epithelium are needed. Our work did discount the likelihood that pancreatic epithelial architecture could be altered in the absence of Rab11 simply due to cell proliferation alone, as we observe no differences in pHH3 expression between control and Rab11 mutant pancreata (Fig. S6 D). In addition, given that *Rab11*^{pancDKO} postnatal islets appear largely normal in their size, number and endocrine cell type composition, we discounted potential cell death as a result of loss of Rab11 (Fig. S7 J-O). At this point, we leave open the possibility that failure of normal glucose tolerance might be impacted directly by the absence of Rab11 in adult endocrine cells, as Rab11 is known to play roles in insulin secretion (Sugawara et al., 2009). Future studies will be needed to address this possibility.

3.5. Rab11 plays a critical role in de novo lumen formation in multiple organs

The mechanisms discovered in this study regarding pancreatic lumen formation likely apply beyond the early pancreas. Indeed, *de novo* lumen formation has been described in other systems (reviewed in Sigurbjornsdottir et al. (2014)), such as the fly trachea (Jazwinska et al., 2003), the worm excretory cells (Khan et al., 2013; Kolotuev et al., 2013), the zebrafish intestine (Alvers et al., 2014), Kupffer's vesicle (Rathbun et al., 2020), and vasculature (Herwig et al., 2011). In zebrafish Kupffer's vesicle, it was shown that Rab11 colocalizes with Par3/aPKC-containing polarity complexes on endosomes and is required for vesicle transport of components to cytokinectic bridges (remnants of abscission required for lumen formation) (Rathbun et al., 2020). In the zebrafish gut tube, Rab11 is critical for trafficking apical proteins to the luminal surface to allow fusion of multiple lumens into a single central gut lumen (Alvers et al., 2014). Hence, our study supports the consensus role of Rab11 as a key mediator of single epithelial lumen formation across species, but demonstrates its requirement for the first time during mammalian organogenesis and during pancreas development.

3.6. Exocrine anatomy and function also depend on Rab11

The exocrine machinery of the pancreas similarly depends on faithful epithelial morphogenesis and lumen formation. Our data show that normal acinar and ductal fate is tied to coordination of epithelial cells to form pre-acinar tips of a certain size. Loss of Rab11 leads to smaller tips and disconnected ducts. These defects persist after birth, when viability of pups is impaired. Whether postnatal survival is primarily driven by the decrease in endocrine mass observed at E14.5, or by the likely decrease in digestive enzyme secretion resulting from a disconnected pancreatic tree is unclear, but we speculate that both are at least partially responsible.

3.7. Summary

Altogether, our findings provide novel insights into the mysteries of pancreatic morphogenesis and lumen formation. We posit that loss of Rab11 blocks vesicles from efficiently returning to the plasma membrane from recycling endosomes, resulting in failure of directional trafficking within epithelial cells, as well as in defects in cell polarity (demonstrated by multiple apical membrane initiation sites per cell) and in junction remodeling. These cellular changes, in turn, result in failure of lumen formation and connection, as well as severely disrupted epithelial morphogenesis. As we have previously shown (Azizoglu et al., 2017), such disruptions of the pancreatic plexus impact normal endocrine differentiation. This study opens the door to closer scrutiny of pancreatic morphogenesis, the importance of which cannot be understated given the growing between the mechanisms of developmental morphogenesis and disease. In the future, we hope to utilize this mutant and others to build a complete picture of pancreatic morphogenesis and to continue elucidating the links between lumen formation and morphogenesis.

4. Materials and methods

4.1. Mouse and embryo handling

All animal husbandry was performed in accordance with protocols approved by the University of Texas Southwestern Medical Center Institutional Animal Care and Use Committee. Both male and female E10.5-E18.5 embryos and postnatal tissues were collected and dissected in PBS. Tissues and embryos were photographed at dissection with a ZEISS NeoLumar S 0.8x FWD 80 mm Microscope, and embryos, pups and adults were photographed with an iPhone12. Tissues were fixed in 4% paraformaldehyde (PFA) in PBS overnight at 4 °C. CD1 or mixed-background littermates were used as controls. *Rab11A*$^{f/f}$, *Rab11B*$^{-/-}$, and *Pdx1-Cre* lines were used in this study (D'Agostino et al., 2019; Yu et al., 2014a). We originally attempted to generate *Rab11*^{pancDKO} mutants by crossing *Rab11A*$^{f/f}$;*Rab11B*$^{-/-}$ females with *Rab11A*$^{f/f}$;*Rab11B*$^{-/-}$;*Pdx1-Cre* males. While the few surviving *Rab11*^{pancDKO} males were viable and fertile, the defects associated with these mutations applied selective pressure and blocked the effective recombination of the *Rab11A* flox sites by the Cre. Subsequently, males were maintained as *Rab11A*$^{f/+}$;*Rab11B*$^{-/-}$;*Pdx1-Cre* or *Rab11A*$^{f/f}$;*Rab11B*$^{+/-}$;*Pdx1-Cre* and bred to *Rab11A*$^{f/f}$;*Rab11B*−/− females to generate *Rab11*^{pancDKO} tissue.

To monitor survival in postnatal mutants, cages with plugged females were monitored from E18.5 to what would be E22.5 for the birth of a new litter. Due to a high frequency of cannibalism, the number of pups was estimated at P0 with minimal perturbations to the cage. Pups were then counted and photographed every day until P8 to track any deaths or failures to thrive. If dead pups were observed in the cage, tissue was collected for genotyping. Toes from live pups were collected for genotyping between approximately P5 and P9, and then mice were weaned between P21 and P28. At weaning, mice were weighed in a cup using a Kitchen Tour Digital Touch scale and photographed using an iPhone 12.

4.2. Glucose tolerance assay

To test the glucose tolerance of adult mice, mice were fasted for at least 12 h (overnight). Mice were then weighed and the appropriate dose of glucose (D+ glucose, Sigma G8270) was calculated (2 mg glucose/g body weight). A baseline blood glucose reading was taken using a True Balance glucometer with True Balance test strips. A fresh razor blade was used to cut off a small piece of the end of the tail, and blood was collected as a bolus that was directly applied to the test strip. Mice were then injected with glucose intraperitoneally, and their blood glucose levels were measured at 15, 30, 60 and 120 min. These values were plotted in PRISM (GraphPad) and analyzed by 2way ANOVA.

4.3. Immunofluorescence on sections

After fixation, tissues were rinsed thrice in PBS then dehydrated via an ethanol gradient and washed twice for 30 min in 100% ethanol. Either immediately or after storage at −20 °C, tissues were cleared by washing in xylene twice for 10 min and then transitioned into paraplast (McCormick Scientific) by washing in 1:1 xylene:paraplast for 10min at 60 °C. Tissues were subsequently washed approximately once per hour for at least 3 h and soaked overnight in paraplast at 37 °C. Tissues were embedded in paraplast and sectioned at either 10uM or 20uM with a Biocut 2030 microtome (Leica) or a HistoCore MULTICUT semi-automated rotary microtome onto SuperfrostPlus glass slides (Fisher).

As previously described (Azizoglu et al., 2017), sectioned tissue was deparaffinized with xylene and then rehydrated through an ethanol series. Sections were permeabilized for 10 min in 0.3% Triton X-100 in PBS then subjected to antigen retrieval with either R buffer A (nuclear antigens) or R buffer B (cytoplasmic antigens) in a 2100 Retriever (Electron Microscopy Services). Slides were blocked with 5% Normal Donkey Serum (NDS) in PBS for 2 h, then incubated in primary antibody diluted in 5% NDS overnight at 4 °C (Table S1). The next day, slides were washed in PBS and incubated in secondary antibody diluted in 5% NDS for 2 h (all secondary antibodies were conjugated to AlexaFluor). Slides were subsequently washed in PBS and blood cells were lysed by a 15 min incubation in 10 mM $CuSO_4$, 50 mM NH_4Cl @ pH = 5 solution, followed by a 5 min wash in H_2O. Finally, slides were washed in PBS and mounted with DAPI Fluoromount-G (Southern Biotech). Stained slides were imaged on a Nikon A1R confocal microscope provided by the UT Southwestern Molecular Biology Department.

For antigens requiring additional antigen retrieval (alternative protocol mentioned in Fig. S2 B,B′), Tyramide signal amplification was performed in accordance with the manufacturer's protocol (Life Technologies) and as previously described (Braitsch et al., 2019).

4.4. Whole-mount immunofluorescence

As previously described (Daniel et al., 2018), fixed tissues were dehydrated to 100% methanol via a gradient and stored at −20 °C until use or transferred directly from PBS to 100% ice cold methanol for a secondary fixation for 30 min at room temperature (RT) and then washed back to PBS via a gradient. Once rehydrated, tissues were permeabilized for 1.5–2 h for tissue between E10.5 and E12.5, 3 h for E14.5 and 4 h for E18.5 tissues and then blocked in CAS Block (ThermoFisher) for at least 2 h. Samples were incubated in primary antibody diluted 1:500 in CAS Block overnight at 4 °C and were washed in PBS at RT for at least 6 h the next day before incubating in secondary antibody diluted 1:500 in CAS Block overnight at 4 °C. Tissues were then dehydrated into 100% methanol and cleared in a 1:2 mixture of benzyl alcohol/benzyl benzoate (BABB) for at least 10 min at RT. Samples in BABB were visualized in concave glass slides using an LSM710 Meta Zeiss confocal provided by the UT Southwestern Molecular Biology Department.

4.5. Single-cell RNA-Sequencing analysis

Single-cell RNA-Sequencing datasets of the developing pancreas at E12.5, E14.5, and E17.5 were reported by (Byrnes et al., 2018)and are available for download at the Gene Expression Omnibus (GEO) (accession number GSE101099). The gene barcode matrices were analyzed with the R package Seurat v3.2.3. High-quality cells were retained by filtering on the number of expressed genes and on mitochondrial content. Each sample was normalized with NormalizeData(), and variable genes were identified with the FindVariableFeatures() function using 2000 genes and the "vst" selection method. Integration anchors were then found for each timepoint with FindIntegrationAnchors() with 30 principle components and 2,00 highly variable genes. All samples for each individual timepoint were then merged, resulting in three separate merged datasets (E12.5, E14.5, and E17.5). Each merged dataset was then scaled with ScaleData and principal component analysis was performed with 30 principal components for each merged dataset. Dimensionality reduction and clustering was performed with FindNeighbors, FindClusters, and RunUMAP on 30 principal components and a resolution parameter of 0.2. The resulting clusters were then annotated as representing known broad cell types based on known markers for each cell type, as described in (Byrnes et al., 2018). Tabula Muris data for *Rab11a* and *Rab11b* expression was extracted by applying the 'FACS' method on the pancreas sample at https://tabula-muris.ds.czbiohub.org/ .

4.6. Cell polarity quantifications

A 'polarity index' for individual cells was generated and quantified on E14.5 tissue sections stained with anti-Laminin (basement membrane), DAPI (nuclei), anti-GM130 (Golgi marker) and an apical marker (often anti-Muc1). Cells were only measured if they were clearly a part of an acinar tip (ductal cells were excluded to the best of our abilities). The "Angle" tool in Fiji was used to manually draw an angle from the Laminin to the GM130 signal (passing through the nucleus), and then from GM130 to the apical marker (Fig. 7 E). The starting point on the basement membrane was selected as the region aligned with the center of the nucleus, and the line drawn from the laminin to the GM130 created an approximate 90° angle from the line to the laminin. Similarly, the line from GM130 to the apical membrane was drawn so the line contacted the closest point of the apical membrane at an approximate 90° angle. If a single cell had more than one apical membrane site, the measurements were repeated for each apical membrane site starting from the same laminin and GM130 locations (Fig. 7 E′). The raw values were then subtracted from 180° (the perfect ideal for a polarized cell) and the absolute value was calculated. Values were manually binned into 10° bins for ease of data representation in Excel. The degree of variation from 180° was then plotted and analyzed via 2-way ANOVA in PRISM.

4.7. Cell-cell junction and polarity marker quantifications

The number of concentrated patches of junction markers (ZO-1) and polarity markers (Par3, Par6b, aPKC, Crumbs3) were manually counted in individual pancreatic epithelial cells (ECad+). The expectation for a perfectly polarized cell was used as the baseline for comparison – for junction markers, there should be two punctae of strong signal on either side of an apical membrane patch, while for apical markers there should only be one region of strong signal per cell on the plasma membrane. These counts were then displayed as the number of ectopic junctional or apical sites per single control or DKO cell. Results were graphed and analyzed via ANOVA in PRISM.

4.8. Lumen discontinuity quantifications

Whole-mount immunofluorescent images of pancreata stained for ECad and Muc1 were loaded into the image analysis program IMARIS. A surface of ECad (detail level 10 μm to reflect the approximate size of a single cell) was created to quantify the total volume of each pancreas. A surface of Muc1 (detail level 2.5 μm) was created, and then the largest volume object (the primary central plexus of connected lumens) was deleted. The number and volume of lumens disconnected from the central plexus were quantified. These values were normalized to the volume of each pancreas in Excel and then plotted and analyzed by Student's t-test in PRISM.

4.9. Pancreatic lineage volume quantifications

Whole-mount immunofluorescent images of pancreata stained for ECad and a lineage marker (Insulin & Glucagon; CPA1; Sox9) were loaded into the image analysis program IMARIS. A surface of a manually-determined Region of Interest (ROI) of ECad signal (detail level 2.5 μm) was created to quantify the total volume of each pancreas (other parameters were determined automatically by IMARIS). Dorsal pancreas only was measured, with the cutoff point for ROI determination being where the tissue is most narrow before expanding into the ventral pancreas. Another surface of the lineage marker (detail level 2.5 μm) using the same ROI was created to quantify the volume of that cell population within the pancreas (other parameters were determined automatically by IMARIS). The sums of the volume measurements for each surface were recorded in excel. Lineage volumes were standardized to the total volume of the individual epithelium, and those values were plotted and analyzed by Student's t-test in PRISM.

4.10. Number of cells per field of view quantification

To quantify morphological changes in the acinar cell compartment, cells as viewed by immunofluorescence in section were determined to be of acinar fate by CPA1 immunofluorescent staining of tissue sections. Using the "Cell Counter" function in FIJI, the number of cells per acinar cluster at E14.5 and the total number of $CPA1^+/pHH3^+$ cells, $CPA1^+$ cells, $pHH3^+$ cells, $ECad^+$ cells, and acini were quantified. This was done for all fully visible acinar rosettes in at least three fields of view of three sections of each biological replicate. These values were plotted and analyzed by Student's T-Test in PRISM.

4.11. Data analysis and visualization

Data were both analyzed and plotted in PRISM 9 XML. Statistical tests (indicated in the relevant methods sections and figure legends) utilized were the parametric unpaired Student's t-test and the 2-Way ANOVA with Tukey's multiple comparisons test ("compare cell means regardless of rows and columns"). ns = $p>0.05$; * = $0.01<p<0.05$; ** = $0.001<p<0.01$; *** = $0.0001<p<0.001$; **** = $p<0.0001$. Images were manipulated in FIJI. Figures and models were made using Microsoft Powerpoint, data were partially analyzed in Microsoft Excel and text was written in Microsoft Word.

Author contributions

Conceptualization: H.R.B., D.B.A., D.M., O.C.; Methodology: H.R.B., D.M., O.C.; Validation: H.R.B., T.B., L.F.; Investigation: H.R.B.; Resources: H.R.B., N.G., O.C.; Data curation: H.R.B., S.D., J.B.S., D.M., O.C.; Writing – original draft: H.R.B., O.C.; Writing – review and editing: H.R.B., D.M., N.A., T.B., N.G, J.B.S., O.C.; Visualization: H.R.B.; Supervision: O.C., D.M.; Project administration: O.C.; Funding acquisition: O.C., H.R.B.

Funding

This work was supported by the National Institute of Diabetes and Digestive and Kidney Diseases (DK106743, DK079862 to O.C.); and an NSF (Graduate Research Fellowship) (2019241092 to H.R.B.). We also acknowledge grants to J.B.S. from the NIH/NIDDK (R01DK118421) and the Nora Eccles Treadwell Foundation. S.D. was supported by the UCSF Discovery Fellows Program, NIH NIGMS IMSD Grant R25GM056847-23, and NIH/NIDDK diversity supplement R01DK118421-02S1. Deposited in PMC for release after 12 months.

Declaration of competing interest

The authors have no competing interests to declare.

Data availability

Data will be made available on request.

Acknowledgements

We would like to thank the entire Cleaver lab, as well as Drs. Elizabeth Chen, Michael Dellinger, Caitlin Maynard and Neal Alto, for discussion and critiques throughout this study. We also acknowledge the support of the UT Southwestern HistoPathology Core for embedding and sectioning of adult tissues.

Appendix A. Supplementary data

Supplementary data to this article can be found online at https://doi.org/10.1016/j.ydbio.2023.05.002.

References

Alvers, A.L., Ryan, S., Scherz, P.J., Huisken, J., Bagnat, M., 2014. Single continuous lumen formation in the zebrafish gut is mediated by smoothened-dependent tissue remodeling. Development 141, 1110–1119.
Andrew, D.J., Ewald, A.J., 2010. Morphogenesis of epithelial tubes: insights into tube formation, elongation, and elaboration. Dev. Biol. 341, 34–55.
Azizoglu, D.B., Braitsch, C., Marciano, D.K., Cleaver, O., 2017. Afadin and RhoA control pancreatic endocrine mass via lumen morphogenesis. Genes Dev. 31, 2376–2390.
Bankaitis, E.D., Bechard, M.E., Wright, C.V., 2015. Feedback control of growth, differentiation, and morphogenesis of pancreatic endocrine progenitors in an epithelial plexus niche. Genes Dev. 29, 2203–2216.
Barry, D.M., Koo, Y., Norden, P.R., Wylie, L.A., Xu, K., Wichaidit, C., Azizoglu, D.B., Zheng, Y., Cobb, M.H., Davis, G.E., Cleaver, O., 2016. Rasip1-Mediated rho GTPase signaling regulates blood vessel tubulogenesis via nonmuscle myosin II. Circ. Res. 119, 810–826.
Braitsch, C.M., Azizoglu, D.B., Htike, Y., Barlow, H.R., Schnell, U., Chaney, C.P., Carroll, T.J., Stanger, B.Z., Cleaver, O., 2019. LATS1/2 suppress NFkappaB and aberrant EMT initiation to permit pancreatic progenitor differentiation. PLoS Biol. 17, e3000382.
Bryant, D.M., Datta, A., Rodriguez-Fraticelli, A.E., Peranen, J., Martin-Belmonte, F., Mostov, K.E., 2010. A molecular network for de novo generation of the apical surface and lumen. Nat. Cell Biol. 12, 1035–1045.
Byrnes, L.E., Wong, D.M., Subramaniam, M., Meyer, N.P., Gilchrist, C.L., Knox, S.M., Tward, A.D., Ye, C.J., Sneddon, J.B., 2018. Lineage dynamics of murine pancreatic development at single-cell resolution. Nat. Commun. 9, 3922.
Camelo, C., Luschnig, S., 2021. Cells into tubes: molecular and physical principles underlying lumen formation in tubular organs. Curr. Top. Dev. Biol. 143, 37–74.
D'Agostino, L., Nie, Y., Goswami, S., Tong, K., Yu, S., Bandyopadhyay, S., Flores, J., Zhang, X., Balasubramanian, I., Joseph, I., Sakamori, R., Farrell, V., Li, Q., Yang, C.S., Gao, B., Ferraris, R.P., Yehia, G., Bonder, E.M., Goldenring, J.R., Verzi, M.P., Zhang, L., Ip, Y.T., Gao, N., 2019. Recycling endosomes in mature epithelia restrain tumorigenic signaling. Cancer Res. 79, 4099–4112.
Daniel, E., Azizoglu, D.B., Ryan, A.R., Walji, T.A., Chaney, C.P., Sutton, G.I., Carroll, T.J., Marciano, D.K., Cleaver, O., 2018. Spatiotemporal heterogeneity and patterning of developing renal blood vessels. Angiogenesis 21, 617–634.
Dekan, G., Gabel, C., Farquhar, M.G., 1991. Sulfate contributes to the negative charge of podocalyxin, the major sialoglycoprotein of the glomerular filtration slits. Proc. Natl. Acad. Sci. U. S. A. 88, 5398–5402.
Desclozeaux, M., Venturato, J., Wylie, F.G., Kay, J.G., Joseph, S.R., Le, H.T., Stow, J.L., 2008. Active Rab11 and functional recycling endosome are required for E-cadherin trafficking and lumen formation during epithelial morphogenesis. Am. J. Physiol. Cell Physiol. 295, C545–C556.
Dong, Q., Fu, L., Zhao, Y., Du, Y., Li, Q., Qiu, X., Wang, E., 2017. Rab11a promotes proliferation and invasion through regulation of YAP in non-small cell lung cancer. Oncotarget 8, 27800–27811.
Flasse, L., Schewin, C., Grapin-Botton, A., 2021. Pancreas morphogenesis: branching in and then out. Curr. Top. Dev. Biol. 143, 75–110.
Gao, L., Yang, Z., Hiremath, C., Zimmerman, S.E., Long, B., Brakeman, P.R., Mostov, K.E., Bryant, D.M., Luby-Phelps, K., Marciano, D.K., 2017. Afadin orients cell division to position the tubule lumen in developing renal tubules. Development 144, 3511–3520.
Goldenring, J.R., Smith, J., Vaughan, H.D., Cameron, P., Hawkins, W., Navarre, J., 1996. Rab11 is an apically located small GTP-binding protein in epithelial tissues. Am. J. Physiol. 270, G515–G525.
Hales, C.M., Vaerman, J.P., Goldenring, J.R., 2002. Rab11 family interacting protein 2 associates with Myosin Vb and regulates plasma membrane recycling. J. Biol. Chem. 277, 50415–50421.
Harland, R.M., 1994. Neural induction in Xenopus. Curr. Opin. Genet. Dev. 4, 543–549.
Herwig, L., Blum, Y., Krudewig, A., Ellertsdottir, E., Lenard, A., Belting, H.G., Affolter, M., 2011. Distinct cellular mechanisms of blood vessel fusion in the zebrafish embryo. Curr. Biol. 21, 1942–1948.
Hick, A.C., van Eyll, J.M., Cordi, S., Forez, C., Passante, L., Kohara, H., Nagasawa, T., Vanderhaeghen, P., Courtoy, P.J., Rousseau, G.G., Lemaigre, F.P., Pierreux, C.E., 2009. Mechanism of primitive duct formation in the pancreas and submandibular glands: a role for SDF-1. BMC Dev. Biol. 9, 66.
Hingorani, S.R., Petricoin, E.F., Maitra, A., Rajapakse, V., King, C., Jacobetz, M.A., Ross, S., Conrads, T.P., Veenstra, T.D., Hitt, B.A., Kawaguchi, Y., Johann, D., Liotta, L.A., Crawford, H.C., Putt, M.E., Jacks, T., Wright, C.V., Hruban, R.H., Lowy, A.M., Tuveson, D.A., 2003. Preinvasive and invasive ductal pancreatic cancer and its early detection in the mouse. Cancer Cell 4, 437–450.
Howe, E.N., Burnette, M.D., Justice, M.E., Schnepp, P.M., Hedrick, V., Clancy, J.W., Guldner, I.H., Lamere, A.T., Li, J., Aryal, U.K., D'Souza-Schorey, C., Zartman, J.J., Zhang, S., 2020. Rab11b-mediated integrin recycling promotes brain metastatic adaptation and outgrowth. Nat. Commun. 11, 3017.
Jazwinska, A., Ribeiro, C., Affolter, M., 2003. Epithelial tube morphogenesis during Drosophila tracheal development requires Piopio, a luminal ZP protein. Nat. Cell Biol. 5, 895–901.
Kesavan, G., Sand, F.W., Greiner, T.U., Johansson, J.K., Kobberup, S., Wu, X., Brakebusch, C., Semb, H., 2009. Cdc42-mediated tubulogenesis controls cell specification. Cell 139, 791–801.
Khan, L.A., Zhang, H., Abraham, N., Sun, L., Fleming, J.T., Buechner, M., Hall, D.H., Gobel, V., 2013. Intracellular lumen extension requires ERM-1-dependent apical membrane expansion and AQP-8-mediated flux. Nat. Cell Biol. 15, 143–156.

Kim, M., A, M.S., Ewald, A.J., Werb, Z., Mostov, K.E., 2015. p114RhoGEF governs cell motility and lumen formation during tubulogenesis through a ROCK-myosin-II pathway. J. Cell Sci. 128, 4317–4327.
Kolotuev, I., Hyenne, V., Schwab, Y., Rodriguez, D., Labouesse, M., 2013. A pathway for unicellular tube extension depending on the lymphatic vessel determinant Prox1 and on osmoregulation. Nat. Cell Biol. 15, 157–168.
Lapierre, L.A., Dorn, M.C., Zimmerman, C.F., Navarre, J., Burnette, J.O., Goldenring, J.R., 2003. Rab11b resides in a vesicular compartment distinct from Rab11a in parietal cells and other epithelial cells. Exp. Cell Res. 290, 322–331.
Marciano, D.K., 2017. A holey pursuit: lumen formation in the developing kidney. Pediatr. Nephrol. 32, 7–20.
Meng, Y., Cai, K.Q., Moore, R., Tao, W., Tse, J.D., Smith, E.R., Xu, X.X., 2017. Pten facilitates epiblast epithelial polarization and proamniotic lumen formation in early mouse embryos. Dev. Dynam. 246, 517–530.
Moreno, M.R., Boswell, K., Casbolt, H.L., Bulgakova, N.A., 2022. Multifaceted control of E-cadherin dynamics by Adaptor Protein Complex 1 during epithelial morphogenesis. Mol. Biol. Cell 33, ar80.
Mostov, K.E., Deitcher, D.L., 1986. Polymeric immunoglobulin receptor expressed in MDCK cells transcytoses IgA. Cell 46, 613–621.
Neto, H., Balmer, G., Gould, G., 2013. Exocyst proteins in cytokinesis: regulation by Rab11. Commun. Integr. Biol. 6, e27635.
Ossipova, O., Kim, K., Lake, B.B., Itoh, K., Ioannou, A., Sokol, S.Y., 2014. Role of Rab11 in planar cell polarity and apical constriction during vertebrate neural tube closure. Nat. Commun. 5, 3734.
Overeem, A.W., Bryant, D.M., van, I.S.C., 2015. Mechanisms of apical-basal axis orientation and epithelial lumen positioning. Trends Cell Biol. 25, 476–485.
Peshavaria, M., Larmie, B.L., Lausier, J., Satish, B., Habibovic, A., Roskens, V., Larock, K., Everill, B., Leahy, J.L., Jetton, T.L., 2006. Regulation of pancreatic beta-cell regeneration in the normoglycemic 60% partial-pancreatectomy mouse. Diabetes 55, 3289–3298.
Pictet, R.L., Clark, W.R., Williams, R.H., Rutter, W.J., 1972. An ultrastructural analysis of the developing embryonic pancreas. Dev. Biol. 29, 436–467.
Pollack, A.L., Barth, A.I., Altschuler, Y., Nelson, W.J., Mostov, K.E., 1997. Dynamics of beta-catenin interactions with APC protein regulate epithelial tubulogenesis. J. Cell Biol. 137, 1651–1662.
Pollack, A.L., Runyan, R.B., Mostov, K.E., 1998. Morphogenetic mechanisms of epithelial tubulogenesis: MDCK cell polarity is transiently rearranged without loss of cell-cell contact during scatter factor/hepatocyte growth factor-induced tubulogenesis. Dev. Biol. 204, 64–79.
Rathbun, L.I., Colicino, E.G., Manikas, J., O'Connell, J., Krishnan, N., Reilly, N.S., Coyne, S., Erdemci-Tandogan, G., Garrastegui, A., Freshour, J., Santra, P., Manning, M.L., Amack, J.D., Hehnly, H., 2020. Cytokinetic bridge triggers de novo lumen formation in vivo. Nat. Commun. 11, 1269.
Ren, M., Xu, G., Zeng, J., De Lemos-Chiarandini, C., Adesnik, M., Sabatini, D.D., 1998. Hydrolysis of GTP on rab11 is required for the direct delivery of transferrin from the pericentriolar recycling compartment to the cell surface but not from sorting endosomes. Proc. Natl. Acad. Sci. U. S. A. 95, 6187–6192.
Roland, J.T., Bryant, D.M., Datta, A., Itzen, A., Mostov, K.E., Goldenring, J.R., 2011. Rab GTPase-Myo5B complexes control membrane recycling and epithelial polarization. Proc. Natl. Acad. Sci. U. S. A. 108, 2789–2794.
Roman-Fernandez, A., Bryant, D.M., 2016. Complex polarity: building multicellular tissues through apical membrane traffic. Traffic 17, 1244–1261.
Rugendorff, A., Younossi-Hartenstein, A., Hartenstein, V., 1994. Embryonic origin and differentiation of the Drosophila heart. Rouxs Arch Dev Biol 203, 266–280.
Ryan, A.R., Cleaver, O., 2022. Plumbing our organs: lessons from vascular development to instruct lab generated tissues. Curr. Top. Dev. Biol. 148, 165–194.
Samakovlis, C., Hacohen, N., Manning, G., Sutherland, D.C., Guillemin, K., Krasnow, M.A., 1996. Development of the Drosophila tracheal system occurs by a series of morphologically distinct but genetically coupled branching events. Development 122, 1395–1407.
Schottenfeld-Roames, J., Rosa, J.B., Ghabrial, A.S., 2014. Seamless tube shape is constrained by endocytosis-dependent regulation of active Moesin. Curr. Biol. 24, 1756–1764.
Sigurbjornsdottir, S., Mathew, R., Leptin, M., 2014. Molecular mechanisms of de novo lumen formation. Nat. Rev. Mol. Cell Biol. 15, 665–676.
Slack, J.M., 1995. Developmental biology of the pancreas. Development 121, 1569–1580.
Stenmark, H., Olkkonen, V.M., 2001. The Rab GTPase family. REVIEWS3007 Genome Biol. 2.
Strilic, B., Kucera, T., Eglinger, J., Hughes, M.R., McNagny, K.M., Tsukita, S., Dejana, E., Ferrara, N., Lammert, E., 2009. The molecular basis of vascular lumen formation in the developing mouse aorta. Dev. Cell 17, 505–515.
Sugawara, K., Shibasaki, T., Mizoguchi, A., Saito, T., Seino, S., 2009. Rab11 and its effector Rip11 participate in regulation of insulin granule exocytosis. Gene Cell. 14, 445–456.
Tanasic, D., Berns, N., Riechmann, V., 2022. Myosin V facilitates polarised E-cadherin secretion. Traffic 23, 374–390.
Villasenor, A., Chong, D.C., Henkemeyer, M., Cleaver, O., 2010. Epithelial dynamics of pancreatic branching morphogenesis. Development 137, 4295–4305.
Woichansky, I., Beretta, C.A., Berns, N., Riechmann, V., 2016. Three mechanisms control E-cadherin localization to the zonula adherens. Nat. Commun. 7, 10834.
Xu, J., Lan, L., Bogard, N., Mattione, C., Cohen, R.S., 2011. Rab11 is required for epithelial cell viability, terminal differentiation, and suppression of tumor-like growth in the Drosophila egg chamber. PLoS One 6, e20180.
Yan, Z., Wang, Z.G., Segev, N., Hu, S., Minshall, R.D., Dull, R.O., Zhang, M., Malik, A.B., Hu, G., 2016. Rab11a mediates vascular endothelial-cadherin recycling and controls endothelial barrier function. Arterioscler. Thromb. Vasc. Biol. 36, 339–349.
Yu, S., Nie, Y., Knowles, B., Sakamori, R., Stypulkowski, E., Patel, C., Das, S., Douard, V., Ferraris, R.P., Bonder, E.M., Goldenring, J.R., Ip, Y.T., Gao, N., 2014a. TLR sorting by Rab11 endosomes maintains intestinal epithelial-microbial homeostasis. EMBO J. 33, 1882–1895.
Yu, S., Yehia, G., Wang, J., Stypulkowski, E., Sakamori, R., Jiang, P., Hernandez-Enriquez, B., Tran, T.S., Bonder, E.M., Guo, W., Gao, N., 2014b. Global ablation of the mouse Rab11a gene impairs early embryogenesis and matrix metalloproteinase secretion. J. Biol. Chem. 289, 32030–32043.
Zhang, J., Su, G., Wu, Q., Liu, J., Tian, Y., Liu, X., Zhou, J., Gao, J., Chen, W., Chen, D., Zhang, Z., 2021. Rab11-mediated recycling endosome role in nervous system development and neurodegenerative diseases. Int. J. Neurosci. 131, 1012–1018.